Published in final edited form as:

J Physiol. 2024 January ; 602(1): 113–128. doi:10.1113/JP284894.

Loss of Mitochondrial Ca^{2+} Uptake Protein 3 (MICU3) Impairs Skeletal Muscle Calcium Handling and Exercise Capacity

Barbara Roman[1], **Yusuf Mastoor**[1], **Yingfan Zhang**[2], **Dennis Gross**[1], **Danielle Springer**[3], **Chengyu Liu**[4], **Brian Glancy**[2,4,*], **Elizabeth Murphy**[1,*]

[1]Cardiac Physiology, NHLBI, NIH, Bethesda, MD

[2]Muscle Energetics, NHLBI, NIH, Bethesda, MD

[3]Mouse Phenotyping Core, NHLBI, NIH, Bethesda, MD

[4]Transgenic Core, NHLBI, NIH, Bethesda, MD

Abstract

Mitochondrial calcium ($[Ca^{2+}]m$) plays an essential role in bioenergetics, and loss of $[Ca^{2+}]m$ homeostasis can trigger diseases and cell death in numerous cell types. Ca^{2+} uptake into mitochondria occurs via the mitochondrial Ca^{2+} uniporter (MCU), which is regulated by 3 mitochondrial Ca^{2+} uptake (MICU) proteins localized in the intermembrane space, MICU 1, 2 and 3. We generated a mouse model of systemic MICU3 ablation and examined its physiological role in skeletal muscle. We found that loss of MICU3 led to impaired exercise capacity. When the muscles were directly stimulated there was a decrease in time to fatigue. MICU3 ablation significantly increased the maximal force of the KO muscle and altered fiber type composition with an increase in the ratio of type IIb (low oxidative capacity) to type IIa (high oxidative capacity) fibers. Furthermore, MICU3-KO mitochondria have reduced uptake of Ca^{2+} and increased phosphorylation of pyruvate dehydrogenase (PDH), indicating that KO animals contain less Ca^{2+} in their mitochondria. Skeletal muscle from MICU3-KO mice exhibited lower net oxidation of NADH during electrically stimulated muscle contraction compared with WT. These data demonstrate that MICU3 plays a role in skeletal muscle physiology by setting the proper threshold for $[Ca^{2+}]m$ uptake, which is important for matching energy demand and supply in muscle.

Graphical Abstract

* **co-corresponding authors** .

Disclosure

No conflict of interest.

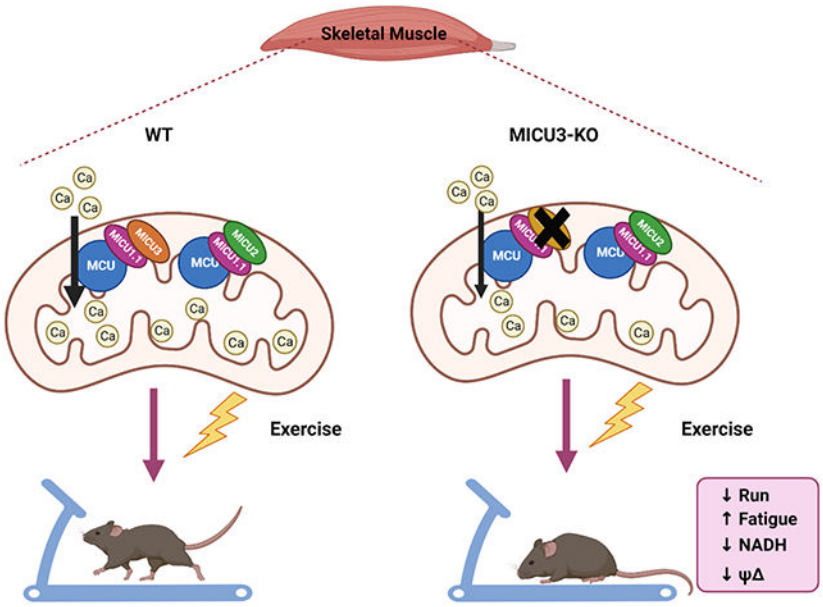

Role of MICU3 in skeletal muscle physiology. Deletion of MICU3 leads to a decline in exercise capacity in mice, along with an accelerated onset of muscle fatigue. The mitochondria from skeletal muscle lacking MICU3 exhibited lower calcium uptake. Furthermore, skeletal muscle from MICU3-KO mice shows reduced net oxidation of nicotinamide adenine dinucleotide (NADH) and membrane potential (ΔΨ) during electrically stimulated muscle contraction in comparison to wild-type (WT) mice. These findings collectively underscore the important role of MICU3 in regulating mitochondrial calcium uptake, which impacts the synchronization of energy demand and supply in skeletal muscle physiology.

Keywords

MICU3; Skeletal muscle; Calcium uptake

Introduction

Mitochondrial Ca^{2+} uptake occurs via the mitochondrial Ca^{2+} uniporter (MCU) (Baughman et al., 2011; De Stefani et al., 2011), which exists in a complex with EF-hand Ca^{2+} binding proteins (Mitochondrial Ca^{2+} Uptake (MICU) proteins). There are 3 MICU proteins, MICU 1, 2, and 3, localized in the intermembrane space (De Stefani et al., 2015; Perocchi et al., 2010; Plovanich et al., 2013; Xing et al., 2019). Only MICU1 can directly bind to MCU, and MICU1 can form either a homodimer or a heterodimer with MICU2 or MICU3 to regulate the Ca^{2+} sensitivity of the MCU (Park et al., 2020). MICU1 homodimers have a lower Kd for Ca^{+2} binding than MICU1-MICU2 heterodimers (Kamer et al., 2017; Park et al., 2020). Thus, replacing MICU1 homodimers with MICU1-MICU2 heterodimers increases the threshold for $[Ca^{2+}]$m uptake (Kamer et al., 2017; Park et al., 2020). Over-expression of MICU3 in Hela cells has been shown to enhance $[Ca^{2+}]$m uptake suggesting that MICU1-MICU3 heterodimers have a reduced threshold for $[Ca^{2+}]$m uptake (Patron et al., 2019).

The MCU and MICU levels and the ratio of MICU1/MCU vary among tissues (Paillard et al., 2017; Tsai et al., 2022). Skeletal muscle also expresses a MICU1 splice variant, MICU1.1 (Reane et al., 2016). While MICU3 is highly expressed in neuronal tissue (Patron et al., 2019), very few studies have examined its role in non-neuronal tissue. A recent study showed that MICU3 protein expression levels significantly increase in skeletal muscle during development (Kim et al., 2019). Compared to postnatal day 1, MICU3 increases ~2-fold by day 7 and 2.6-fold by day 21. Interestingly, MCU and MICU1 decrease postnatally in skeletal muscle. By postnatal day 21, MICU1 decreases to 40% of its level at postnatal day 1, and MCU decreases to 50% of postnatal day 1 levels (Kim et al., 2019). Additionally, with aging, there is a loss of skeletal muscle mass, and a recent study showed a concomitant decrease in MICU3 in skeletal muscle along with the loss of muscle. It also was shown that restoring the levels of MICU3 in aged skeletal muscle reversed muscle dysfunction, suggesting a role for MICU3 in regulating skeletal muscle function (Yang et al., 2021). To further investigate the role of MICU3, we studied a mouse model with a systemic lack of MICU3 and showed that loss of MICU3 reduced cardiac dysfunction following isoproterenol induced hypertrophy (Puente et al., 2020). In this study we examined the role of MICU3 in skeletal muscle and found that loss of MICU3 led to a decrease in exercise capacity and in time to fatigue. We also found that loss of MICU3 led to altered fiber type composition with an increase in the ratio of type IIb (low oxidative capacity) to type IIa (high oxidative capacity) fibers. Furthermore, mitochondria that lack MICU3 exhibited a net oxidation of NADH during electrically stimulated muscle contractions. Taken together, these data suggest that MICUs levels are regulated in a tissue- specific manner which is important for tissue-specific function.

Methods

Ethical Approval.

All animal protocol were approved by the National Heart, Lung, and Blood Institute Animal Care and Use Committee (HL-0177) and adhered to the Animal Care and Welfare Act directives.

Animals.

The mitochondrial calcium uptake 3 (MICU3) knockout (KO) mice were generated using the CRISPR-Cas9 (clustered regularly interspaced short palindromic repeat–associated 9) method (Puente et al., 2020; Wang et al., 2013). Briefly, two single guide RNAs (sgRNAs) were designed to delete the MICU3 gen, one guide binds to the coding region of Exon1 (CGGCTCCCGGGATGTCGGGC) and the other to Exon 12 (CGTGCTGTATACGTAGCTAC) of the mouse Micu3 genomic DNA. These sgRNAs were synthesized using ThermoFisher's sgRNA In Vitro Transcription service, and were co-microinjected at 20ug/ml together with Cas9 mRNA (50 ug/ml, TriLink BioTechnologies, San Diego, CA) into the cytoplasm of zygotes collected from C57BL/6N mice (Charles River Laboratory). Injected embryos were cultured overnight in KSOM medium (Millipore Sigma) in a 37°C incubator with 6% CO2. The next morning, embryos which reached the 2-cell stage of development were implanted into the oviducts of pseudo pregnant surrogate mothers (CD1 mice from Charles River Laboratory). Offspring born to the foster mothers

were genotyped using PCR followed by Sanger sequencing. It was produced a mice with a knockout mutation with the entire region between Exon1 and Exon 12 deleted. The mice were used in this study (Ex1–12) and they clearly lack the expression of the MICU3 protein (Figure 1A).

All animal experiments were performed following the guidelines of the Guide for the Care and Use of Laboratory Animals (National Institutes of Health), and all animal protocols were approved by the National Heart, Lung and Blood Institute's Animal Care and Use Committee. The mice used in these experiments were between 3 and 6 months old and included both males and females. The animals were provided with *ad libitum* access to food. For the *in vivo* study to assay of muscle contraction strength mice were anesthetized with isoflurane (using 4–5% Isoflurane with 1 L/min 100% O2) for 1 minute in an induction chamber and then maintained with 2% Isoflurane via a nosecone, when the animals were placed on a heated platform. For tissue harvest and mitochondria isolation mice were anesthetized with intraperitoneal sodium pentobarbital (50 mg/kg) and Heparin (50 USP). After the animals had reached a stage of anesthesia characterized by the loss of the pedal withdrawal reflex, at which point the muscle was harvested and the animal died by exsanguination.

Treadmill running.

Mice were tested for exercise capacity using a Columbus Instruments rodent treadmill (Model Eco-6M), set at a 10-degree incline, as described in (Liu et al., 2020). Mice were acclimated to the walking on the treadmill at a speed of 8–12 m/min for 10 minutes on three consecutive days, and rested one day prior to the test. The testing protocol was as follows: ten min with belt speed at 10 m/min, 12 m/min for five min, 15 m/minute for three minutes. Then, the belt speed was increased incrementally by 1.8 m/min every three min until the mouse became exhausted. Total time, distance, maximum speed, and work were recorded at the time of exhaustion, defined as when mice were unable to continue running without repeatedly falling back onto the shock grid at the back of the treadmill.

In vivo Assay of muscle contraction strength (Isometric torque test).

In vivo muscle contractility was measured in the plantar flexor muscle group (gastrocnemius and soleus) of the lower limb, using an Aurora Scientific Inc model 1300A. Mice were anesthetized using 4–5% Isoflurane with 1 L/min 100% O2 for 1 minute in an induction chamber and then placed supine on a heated platform and maintained with 2% Isoflurane via a nosecone. The knee was kept stationary, and the foot was firmly fixed to a footplate, which was connected to the shaft of the motor. The foot was aligned at 90° to the tibia. Muscle contraction (ankle plantar flexion) was elicited by placing subcutaneous electrodes in the gastrocnemius and soleus. A force frequency protocol was performed by applying a series of stimulation frequencies directly to the plantar flexion muscle group from 25 to 250 Hz at 25-Hz increments with a pause of 1 min between stimuli, and maximal isometric torque (mN-m) was measured at full tetanic contraction at each frequency. After completing the force frequency curve, and a rest period of three minutes, a series of 100 tetanic contractions delivered every five seconds at a stimulation frequency of 150Hz was used to induce muscle

fatigue. The maximal isometric torque measurements were normalized to body weight (kg), which is reported as specific torque (mN-m/kg).

Histology and confocal image.

Soleus and extensor digitorum longus (EDL) muscle were dissected from 6 months old control and KO mice and were embedded in an embedding mold with optimal cutting temperature (O.C.T) compound. The embedded muscle was then immersed in cooled 2-methyl butane of −78 °C for 5 min to freeze the muscle. 10 μm-thick sections of the frozen muscle were acquired with a cryostat (Leica) at −20 °C and collected on room temperature positive charged slides. For immunostaining, the slides were brought to room temperature, and washed three times with 1x PBS solution. The sections were blocked with blocking buffer (1 × PBS containing 5% of goat serum and 1% of bovine serum albumin) for 1 hour and then incubated in blocking buffer containing 0.05% Tween and primary antibodies overnight at 4 °C. The MyHC antibodies (DSHB) used were: BA-D5 (1:60, myosin heavy chain type I), SC-71 (1:100, myosin heavy chain type IIa), and BF-F3 (1:80, myosin heavy chain type IIb). Sections were washed 3 times with 1x PBS containing 0.05% Tween and then incubated in Alexa Fluor or CF dye-conjugated secondary antibodies (Invitrogen) for one hour. The sections were washed 3 times again with 1x PBS containing 0.05% Tween, and coverslips were mounted on the sections with Prolong gold antifade mountant (Life Technologies). Confocal images were collected with a Zeiss LSM 780 confocal microscope system.

Isolation of mitochondria from skeletal muscle.

Mice were euthanized to dissect hind limb muscles (~1.5g). All the procedures were carried out on ice. The isolated muscles from both legs were transferred into ~10 ml isolation medium (150 mM sucrose, 75 mM KCl, 50 mM Tris-HCl, 1 mM KH_2PO_4, 5 mM $MgCl_2$, 1 mM EGTA, pH 7.4). Muscles were minced into small pieces in isolation medium, and 0.5mg Subtilisin A (1mg/ml in isolation buffer, Sigma-Aldrich Cat# P3910) were added. Before homogenization 5 ml of isolation medium containing 0.2% BSA were added. The minced muscle tissue were then homogenized for 15 seconds at 40% of full power with Polytron (IKA Works, INC. Model: Ultra Turrax T25). Homogenized solution was centrifuged at 700g for 10 minutes at 4°C. After the first spin, the supernatant was poured into a clean tube chilled on ice and then spun at 10,000 g for 10 minutes at 4°C. The resulting pellet (mitochondria) was resuspended in Buffer B (225mM Mannitol, 75mM Sucrose, 5mM MOPS, 2mM Taurine, pH 7.25), 0.2% albumin. The enrichment of mitochondria was washed and centrifuged at 11,000 g for 3 min at 4°C. The final mitochondrial pellet was resuspended in 1 ml of Buffer B without albumin to measure mitochondrial protein concentration by Bradford (Thermo Fisher Scientific Cat#1856209).

Measurement of calcium uptake and CRC.

Isolated mitochondria from skeletal muscle were resuspended at a concentration of 0.5 μg/μl in Buffer B. To load mitochondria with Rhod2-AM, we added 2.25μl of 8.9 mM Rhod2-AM (Cayman Chemical, Cat#145037-81-6, final concentration 20μM) to 1ml of 0.5 mg mito/ml. The mitochondria suspension was incubated for 30 mins at room temperature in the dark. After incubation, the mitochondria were centrifuged for 2 min at 11,000g, and washed

gently twice with 1 ml ice-cold buffer B + 0.2% BSA then once with 1 ml Buffer D (KCl 137mM, HEPES 20mM, KH2PO4 2mM, pH 7,2). After the last wash, we resuspended the dye-loaded mitochondria in 0.8 ml Assay Buffer (new Buffer D + 5 mM Glutamate/Malate). Fluorescence was measured at 532-nm excitation and 590nm emission on a ClarioStar plate reader. Experiments were initiated by addition of 5μM CaCl2.

Calcium retention capacity (CRC) assay was performing as previously describe (Parks et al., 2019). To analyzed the uptake and retention of Ca^{2+}, we utilized the fluorescent calcium marker Ca^{2+} Green-5N (1 μM, Molecular Probes Cat#C3737 Invitrogen), a probe designed to quantify extramitochondrial calcium levels. We conducted a series of Ca^{2+} pulses with concentrations ranging from 5 to 10 μM until the opening of the mitochondrial permeability transition pore (PTP), characterized by a sudden increase in the signal. Fluorescence was measured at 485-nm excitation and 530nm emission on a ClarioStar plate reader.

Immunoprecipitation (IP).

Isolated mitochondria from skeletal muscle were incubated on ice for 30 minutes in IP buffer: 50mM Tris, 150mM NaCl, 1% NP-40, 1mM EDTA, Protease & Phosphatase Inhibitors at pH 7.4. A total of 300μg of mitochondria were dissolved in 200μl of IP buffer and incubated with 5μl of anti-MCU antibody (Sigma-Aldrich, #HPA016480) overnight at 4°C with rotation. A control negative of IP was considerer 300μg of mitochondria dissolved in 200μl of IP buffer and incubated with 5μl of anti-IgG antibody. The next day, magnetic beads (Dynabeads, Thermo #10004D) were washed three times with IP buffer and combined with the lysis buffer for 2 hours at room temperature. The immunocomplexes were separated using SDS-2.5% of 2β-Mercaptoethanol and heated at 70°C for 10 minutes. The co-immunoprecipitated proteins were separated by SDS-PAGE gel electrophoresis, transferred to a nitrocellulose membrane, and incubated with anti-MICU1 overnight as explained in the WB section.

Blue Native-Polyacrylamide gel electrophoresis.

Blue Native-Polyacrylamide gel electrophoresis (BN-PAGE) was carried out to study MICU1 in the MCU complex, as previously described (Liu et al., 2020; Reane et al., 2016). Briefly, freshly isolated mitochondria were incubated on ice with Native PAGE sample buffer (Invitrogen Cat#BN2001) and dissolved with DDM (Invitrogen Cat#BN2005) at a final concentration of 0,5%. Crude extract was centrifuged at 4°C, 18000g for 30 minutes, and the protein in the supernatant was quantified using the Bradford method. After that, the proteins were dissolved in 1x Native PAGE sample buffer with Native PAGE 5% G-250 Sample Additive (Invitrogen Cat#BN20041) to a final concentration of 0.25%. 20 μg of proteins were loaded into a 3–12% gel, and electrophoresis running buffers were prepared according to the manufacturer’s protocol for the Native PAGE Novex Bis-Tris Gel System. Once the electrophoretic run was complete, the gels were photographed and transferred to a nitrocellulose membrane using the BioRad system. Thereafter, the membranes were blocked for 2 hours at room temperature and immunoblotted with a primary antibody against MICU1 (1:300, Sigma-Aldrich #HPA016480) at 4°C overnight. The bands were developed by a chemiluminescent as is explain below.

Western blot (WB)

Immunoblotting was performed on RIPA-lysed frozen soleus tissue from both legs. Briefly, the chopped soleus was homogenized in 4 vol of ice-cold RIPA buffer (Thermo #89901, pH 7.4) plus protease inhibitor cocktail (Thermo Scientific, #A32961) using PRECELLYS-24 DUAL (Berting Corp). Then, the homogenate was centrifuged at 10,000g for 15 min at 4°C and the supernatant collected and immediately snap-frozen in liquid N2, and stored at −80°C. The concentration of each soleus sample was quantified by Bradford method (Thermo Scientific #1856209) with bovine serum albumin as the standard. The protein was prepared in 1X LDS NuPAGE loading buffer (Invitrogen, NuPAGE #NP0007) with 2.5% or 10% for MICU3 of 2β-Mercaptoethanol (Sigma #M3148–25ml) without heat. The samples were resolved on SDS-PAGE in NuPAGE 4–12% gradient gel and transferred to a nitrocellulose membrane using BioRad Trans-Blot-Turbo System (7min). Membranes were blocked with 5% nonfat milk in Phosphate-Buffered Saline (pH 7.5) containing 0.1% Tween (PBS-T). For immunological detection of MCU, MICU3, MICU1, MICU2, EMRE, pSer293PDH, PDH and the loading control TOM-20 and GAPDH, the membranes were probed overnight at 4°C with corresponding antibodies: anti-MCU (1:1.000;Sigma-Aldrich #HPA016480), anti-MICU3 (1:250;Sigma-Aldrich #HPA024771), anti-MICU1 (1:1.000;Sigma-Aldrich #HPA037480), anti-MICU2 (1:1.000; Sigma-Aldrich #HPA045511), pSer293PDH (1:1000), PDH (1:1000, Santa Cruz Biotechnology #), anti-TOM-20 (1:2.000; Santa Cruz Biotechnology #(FL-145)sc-11415), anti-EMRE (1:500, Santa Cruz #(C-12) sc-86337) and anti-GAPDH (1:1000, Santa Cruz, #(FL-335) sc-25778). The membranes were washed for 30 min with changes of TBS-T every 10 min before the addition of HRP-conjugated anti-rabbit or mouse secondary antibody for 1hs (1:5,000; Cell Signaling #7074). The bands were developed by a chemiluminescent reagent (ECL Plus; Amersham Biosciences) using the LICOR system to detect the signal. Protein bands were quantified with ImageJ software (NIH) and were analyzed using GraphPad version 9.

RNA isolation, reverse transcriptase reaction, and quantitative Real-Time PCR,

RNA isolation, reverse transcriptase reaction, and quantitative Real-Time PCR, were performed to study the expression patterns of MICU1 and MICU1.1 in skeletal muscle tissues from MICU3-KO and WT mice. We followed the method previously described by (Reane et al., 2016). The Soleus muscle was isolated from the animals, and total RNA was extracted using the RNeasy Mini Kit (Qiagen #74104) following the manufacturer's instructions. RNA concentration was assessed using the Nanodrop instrument (Thermo Fisher Scientific). For retro-transcription, 1 μg of total RNA from each sample was used with the iScript™ cDNA Synthesis Kit (BioRad #1708890). Polymerase chain reaction (PCR) was conducted using a SYBR green PCR kit (Roche #4913914001) and detected with an MX3005P detector from Agilent Technologies. Each reaction was performed in triplicate. The primers used for Real-Time PCR demonstrated an efficiency ranging between 90% to 110%. The housekeeping gene GAPDH was employed as an internal control for cDNA normalization. Expression levels were quantified using the $2^{-\Delta\Delta Ct}$ method. The following table displays the primer sequences used for qPCR:

Target	Primers
MICU1	Fw 5’-GCGCTTTGATGGAAAGAAAATTGC-3’
	Rv 5’-TGTCTACCTCTCCGTCTCCA-3’
MICU1.1 splice variant specific (NM_001291443):	Fw 5’-CTTTGATGGAAAGGAGTTCTGGC-3
	Rv 5’-CCTCCATGTCTACCTCTCCGT-3’
GAPDH	Fw 5’-CACCATCTTCCAGGAGCGAG-3’
	Rv 5’-CCTTCTCCATGGTGGTGAAGAC-3’

Muscle fiber isolation.

Soleus and flexor digitorum brevis (FDB) muscles were dissected in vivo from anaesthetized mice. Skin was surgically removed and the soleus and FDB muscle were detached from the bone at the distal and proximal tendons. Muscle fibers for isolation were digested with 3 mg/ml collagenase D (Sigma, Cat#11088858001) in 1 ml Tyrode buffer (pH = 7.4) containing: 10 mM HEPES, 137 mM NaCl, 4.5 mM KCl, 0.5 mM MgSO4, 0.5 mM KH2PO4, 10 mM glucose, 1.8 mM CaCl2, 1mM Pyruvate and, 10mM BDM at 37°C for 60 min. After digestion, the Collagenase D solution was replaced with fresh Tyrode at 37°C. The fibers were disrupted from the muscle by mechanically pipetting. Once fibers are separated, they were transferred to a new tube and spin down and gently washed two time with Tyrode at 37°C without BDM and then resuspended in 500ul of Tyrode 37°C without BDM for immediately plated onto dishes with Matrigel coating (Corning, NY, USA) containing. NADH and TMRM measurements in isolated fibers were performed 15–30 min after plating cells in the dish.

NADH and membrane potential measurement in isolated muscle fibers.

NADH autofluorescence and mitochondrial energetic flux were evaluated in intact fibers by the mitoRACE method as previously described (Willingham et al., 2019). NADH autofluorescence was imaged in isolated fibers using a Leica SP8 3X STED microscope, a Coherent UV laser tuned to 355nm, a Leica HyD SMD time-gated PMT collecting emission between 400–500nm, and a Leica oil immersion HC PL APO CS2 63x (1.40 NA) objective (Leica Microsystems, Inc., Wetzlar, Germany). For imaging isolated fibers loaded with TMRM (15nM), samples were excited with a pulsed white-light laser tuned to 548nm and emission was read between 565–610nm using a HyD PMT. All images were taken using with a scanning speed of 600Hz, a pixel format of 512×512, and a pinhole size of 1.0 AU. NADH autofluorescence was imaged at rest for 1min to establish baseline signal intensity. Next, NADH intensity was recorded while fibers were stimulated for 1 min at 10Hz and 8V. The fully reduced and maximum NADH intensity signal was acquired by adding 5 mM KCN to the fibers via perfusion resulting in the complete inhibition of oxidative phosphorylation. The average fluorescence intensity was quantified by selecting a region of interest and measuring intensity in that region over time using ImageJ (Bethesda, MD, USA).

NADH autofluorescence was analyzed as a change in the NADH fluorescence response of individual Soleus or FDB muscle fibers during stimulation compared to the baseline. It was calculated as ΔF/F0 (Stimulation-Baseline)/Baseline, and the data were normalized for the maximal value of NADH. Additionally, we calculated the Rate of Increase in NADH fluorescence using mitoRACE (Slope). TMRM fluorescence was also evaluated as a change in ΔF/F0 (Stimulation-Baseline)/Baseline, and the data were normalized by the maximal value of NADH of each fiber.

Statistics.

GraphPad Prims 9, LLC (version 9.5.1) was used for graphics and analysis. All data are expressed as mean (standard deviation measurement (SD)), and differences were tested with either the Student's unpaired t-test (for comparison of 2 groups) or One-way analysis of variance (ANOVA) with Bonferroni correction for datasets with more than two groups. The experiments conducted with cells followed a hierarchical structure and were analyzed using nested t-test (Eisner, 2021). Statistical significance was defined as $P < 0.05$ (95% confidence interval). All data displayed a normal distribution and variance was similar between groups for each evaluation.

Results

Genetic ablation of MICU3 impairs exercise capacity

To test whether MICU3 plays a role in regulating skeletal muscle function, we tested the exercise capacity of WT and MICU3-KO mice. WT and MICU3 mice were run to exhaustion on a treadmill and we observed that MICU3-KO mice ran significantly less than WT mice (WT 827.6 (39.3) vs KO 644.2 (93.3) m; p=0.0037, Figure 1B). We calculated the work and maximal speed for each strain, and found a significant reduction in the MICU3-KO animals (WT 31.2 (1.13) vs KO 28.3 (1.44) Kg.m Figure 1C, (p=0.0065) and WT 4.3 (0.22) vs KO 3.2 (0.55) m/min; p=0.0138, Figure 1D). These differences occurred without a difference in muscle mass (hind limb muscles from both legs, Figure 1E). Taken together these data show that loss of MICU3 impairs exercise capacity.

Changes in the force response and fatigue during *in-vivo* stimulation

To determine whether the impaired exercise capacity was due to a defect in skeletal muscle, we evaluated contractions in the gastrocnemius (GAS) and soleus muscles evoked by direct electrical field stimulation and measured muscle strength and fatigue. Fatigue was evaluated by the administration of a series of tetanic contractions in succession (100Hz). As shown in Figure 2A, intact muscle exhibits a marked force depression with repeated tetanic contractions (500 sec). The loss of 50% of force occurred earlier for the MICU3-KO (182.5 (66.1) sec) than in the WT muscle (253.3 (104.6) sec), consistent with an earlier fatigue in KO than in WT muscles. The force was determined as ankle torsion of GAS and soleus muscle and the data are reported as max/min torque vs. force due to the rotational component. We observed that for each stimulation frequency between 25–250 Hz, the KO mice developed significantly greater force than WT mice (Figure 2B). Altogether, these studies show that loss of MICU3 affected the properties of the force response and fatigue, possibly suggesting muscle fiber switching in the KO animals.

MICU3 deficiency is associated with fiber type switching

An increase in fatigue and force could be explained by a change in fiber-type (Handschin et al., 2007; Watanabe & Wada, 2020). To test this hypothesis, we isolated cryo-sections from soleus muscle and performed immunostaining to identify the different fiber types using antibodies against myosin heavy chain Type I (MHC-I, blue color), IIA (MHC-IIa, green color), and IIb (MHC-IIb, red color). Analysis of these confocal images (Figure 3A–B), indicated that in MICU3-KO muscle type I and type IIa fibers were reduced by 3.52 and 7.43 %, respectively compared with the WT muscle. We also observed a significant increase in type IIb fibers (+11.45%) in soleus muscle from MICU3-KO animals (Figure 3A–B). In WT animals, type IIb fibers were very rarely found in soleus (Figure 3A and C). Thus, soleus muscles of MICU3-KO have a higher percentage of the glycolytic IIb fibers. WT EDL muscle has higher levels of type IIb fibers than soleus and there was no significant change in the MICU3-KO (Figure 3B and D).

Lack of MICU3 leads to an increase in MICU1.1

To better understand the biochemical basis underlying the phenotypic alterations observed in MICU3-KO mice, we used western blotting to examine differences in the regulators of the MCU complex. We tested if MCU, MICU1, MICU2, or EMRE changed in the MICU3-KO soleus muscle. As shown in Figure 4A and B, there is a significant increase in the MICU1/MCU ratio in the KO mice whereas the levels of MICU2/MCU, MCU/TOM20 and EMRE/GAPDH are not different between WT and KO soleus muscle. These data would be consistent with the loss of MICU3 resulting in an increase of MICU1-MICU1 homodimers in the MCU complex in soleus muscle of MICU3-KO.

To determine if the increase in MICU1 corresponded to an increase in MICU1 dimerized with MCU we immunoprecipitated with MCU and probed for MICU1 and found significantly higher levels in KO (Figure 4C). We also ran a non-reducing gel and found more MICU1 in the MCU complex in KO compared to the WT (Figure 4D). Skeletal muscle has a specific MICU1 isoform, MICU1.1. As the antibodies recognized both isoforms, we measured mRNA levels for MICU1 vs MICU1.1 (see Figure 4E). We found that the MICU3-KO muscle had significantly higher expression of MICU1.1 compared to WT. These data suggest that the loss of MICU3 predominantly increases MICU1.1.

Lack of MICU3 leads to a mitochondrial calcium decline

It has been reported that MICU3 enhances $[Ca^{2+}]$m uptake in neuronal tissue (Patron et al., 2019). As the composition of MICUs regulates the sensitivity of MCU to Ca^{2+} (Kamer et al., 2017; Park et al., 2020), we tested whether lack of MICU3 alters mitochondrial calcium uptake in skeletal muscle. Mitochondria from WT and MICU3-KO skeletal muscle from both legs were isolated and loaded with Rhod-2, a calcium-sensitive fluorophore. Pulses of Ca^{2+} (5μM) were added to the Rhod-2 loaded mitochondria and changes in mitochondrial matrix Ca^{2+} due to uptake of extramitochondrial Ca^{2+} were measured by following changes in Rhod-2 fluorescence. Figure 5A shows a representative trace of Rhod-2 fluorescence in WT and KO mitochondria following multiple Ca^{2+} additions. Addition of Ru360 demonstrates that the Ca^{2+} uptake is dependent on MCU. This figure shows that WT mitochondria accumulate more Ca^{2+} than MICU3-KO mitochondria. Data

from 8 biological replicates are summarized in Figure 5B. We also examinate, the Ca^{2+} uptake using Calcium Green-5N to measure extramitochondrial Ca^{2+}. Figures 5C and D show that MICU3-KO mitochondria are able to take up more calcium than WT before undergoing PTP (mitochondrial permeability transition pore). To further assess $[Ca^{2+}]m$, we also measured the levels of phosphorylated PDH (pyruvate dehydrogenase), which has been demonstrated to be inversely proportional to mitochondrial calcium level (Denton et al., 1972; Siess & Wieland, 1972). Figure 5E, shows an increase in phosphorylated PDH in MICU3-KO soleus muscle consistent with lower mitochondrial calcium in KO relative WT. Taken together these data suggest that at baseline MICU3-KO mitochondria have lower mitochondrial calcium than WT.

Metabolic consequences of MICU3 ablation

It has been demonstrated that an increase in work leads to an increase in cytosolic Ca^{2+}, which in turn increases $[Ca^{2+}]m$. This increase in $[Ca^{2+}]m$ has been shown to enhance NADH production, thereby matching energy demand and supply (Liu & O'Rourke, 2008; Wescott et al., 2019). To determine whether the lack of MICU3 alters energy supply and demand matching, we isolated soleus muscle fibers from WT and MICU3-KO mice and measured NADH autofluorescence using one-photon excitation before and after electrical stimulation of the muscle. Mitochondria were also loaded with tetramethyl rhodamine, methyl ester (TMRM) fluorophore to monitor the membrane potential and confirm the mitochondrial localization of the NADH signal in fibers (Figure 6A–C).

We evaluated NADH and TMRM fluorescence at baseline (resting) in isolated soleus skeletal muscle fibers, and then to mimic an increase in work, we electrically stimulated for 1 min at 10Hz. At the end of the study, cyanide was added to provide the fully reduced NADH signal. As shown in a representative trace in Figure 6D, electrical stimulation resulted in no change in NADH fluorescence in the WT soleus muscle; however in MICU3-KO soleus muscle, electrical stimulation resulted in a significant decrease in NADH (−7% decrease, p=0.0351) as shown in Figure 6E. We also evaluated TMRM fluorescence and observe a significant decrease after stimulation in the MICU3-KO but not in the WT fibers (Figure 6F). This indicates that the membrane potential in the KO fibers can become depolarized by stimulation. We also analyzed production of NADH (flux) using mitoRACE (redox after cyanide experiment, (Willingham et al., 2019)). Inhibition of mitochondrial electron transfer chain flux by perfusion of potassium cyanide (5 mM) resulted in an rapid, linear increase in NADH fluorescence at a rate of 3.23 (1.71) % of the total NADH pool per min for WT fibers while MICU3-KO fibers exhibited a lower rate (1.80 (1.76) % NADH m−1) (Figure 6G). We also examined NADH and TMRM in FDB muscle and found a similar response. Upon stimulation NADH does not change in WT FDB muscle, but there is a significant decline in MICU3-KO FDB muscle (Figure 7A–D). Taken together these data suggest that MICU3-KO fibers have reduced generation of NADH compared to WT, which would interfere with energy demand and supply matching.

Discussion

Ca^{2+} uptake into mitochondria is important for regulating cell energetics (Glancy & Balaban, 2012) and cell death (Bauer & Murphy, 2020). Uptake of Ca^{2+} into the mitochondria is thought to be critical for matching NADH redox potential and ATP production to increased energetic demand (Liu & O'Rourke, 2008; Maack & O'Rourke, 2007; Wescott et al., 2019). However, excessive uptake of $[Ca^{2+}]$m can lead to activation of a non-specific channel in the mitochondria and thereby initiate cell death (Bauer & Murphy, 2020). Uptake of Ca^{2+} into mitochondria occurs via the MCU complex (MCUc) (De Stefani et al., 2015). MCU, the pore forming unit is regulated by the MICU family of EF hand Ca^{2+} binding proteins (Matesanz-Isabel et al., 2016; Plovanich et al., 2013). The levels of MICU1 and 2 have been shown to vary between tissue leading to tissue specific regulation of mitochondrial homeostasis (Paillard et al., 2017; Tsai et al., 2022). Tissue specific regulation of $[Ca^{2+}]$m can be important in modulating the energetics of the tissue as well as protecting the cell from Ca^{2+} overload induced cell death. A tissue specific isoform of MICU1.1 has been identified in skeletal muscle (Reane et al., 2016). A number of studies have examined the role of MICU1 and 2 in regulating MCUc in different tissues (Debattisti et al., 2019; Kamer & Mootha, 2014; Paillard et al., 2017; Reane et al., 2016; Shamseldin et al., 2017; Tsai et al., 2022); however there have been few studies investigating the role of MICU3. Patron and co-workers demonstrated in neuronal tissue that MICU3 enhances Ca^{2+} uptake into the mitochondria (Patron et al., 2019). MICU3 has been considered to be a neuronal specific MICU and there has been little study of its role in non-neuronal tissue. The aim of this study was to characterize the role of MICU3 in skeletal muscle.

The data in this study provide evidence suggesting that MICU3 plays an important role in skeletal muscle physiology. MICU3-KO mice are healthy and do not exhibit any adverse phenotype. In fact, previous studies have shown that they are more tolerant of isoproterenol induced cardiac hypertrophy (Puente et al., 2020). The loss of MICU3 does not result in changes in MCU, MICU2 or EMRE, but does result in an increase in MICU1.1, which could be compensatory. Interestingly, the splice variant MICU1.1 binds Ca^{2+} with higher affinity than MICU1 and similar to MICU3 (Reane et al., 2016; Vecellio Reane et al., 2022). It has been shown that $[Ca^{2+}]$m plays a role regulating skeletal muscle trophism (Mammucari et al., 2015); therefore with loss of MICU3, replacement with MICU1.1 is likely to be a compensatory mechanism to maintain Ca^{2+} handling requirements and the mass muscle.

This work provides novel insights showing that loss of MICU3 significantly alters exercise capacity in the skeletal muscle. We observed that KO animals run significantly less than WT, and direct stimulation of the muscle demonstrated that the loss of MICU3 has a direct effect on skeletal muscle. Loss of exercise capacity and fatigue are complex phenotypes and a complete understanding of how a loss of MICU3 leads to these changes will require additional study. The mechanism responsible for the decrease in exercise capacity appears to be due in part to a slight but significant increase in glycolytic IIb fiber type in soleus along with a decrease in mitochondrial Ca^{2+} uptake in the MICU3-KO fibers thereby decreasing generation of NADH which impairs the ability to match energy demand and supply. The loss of MICU3 reduces the increase in $[Ca^{2+}]$m during contraction and this is likely to play a major role in the reduced force generation in the MICU3-KO muscle. The increase

in MICU1.1 is likely to be a compensatory mechanism. The accumulation of $[Ca^{2+}]m$ is hypothesized to be critical for matching NADH redox potential and ATP production to match energy supply and demand. Thus, reduced $[Ca^{2+}]m$ accumulation should impact NADH production in response to increased work. The isolated muscle fibers from WT mice did not show any change in NADH after stimulation consistent with previous studies (Brandes & Bers, 1997; Liu & O'Rourke, 2008). However, MICU3-KO fibers showed a significant decrease in the NADH fluorescence intensity after stimulation, similar to studies in heart using Ru360 to inhibit $[Ca^{2+}]m$ uptake (Liu & O'Rourke, 2008). In addition to measuring changes in NADH redox upon electrical stimulation, we also used mitoRACE to monitor the rate of NADH generation in single cells. Willingham and Glancy studied mitochondrial function *in-vivo* in Tibialis anterior myofibers and found no change in NADH redox between resting and immediately post-stimulation. However, NADH flux rates measured with mitoRACE were significantly higher at post-stimulation than at rest (Willingham et al., 2019). Using mitoRACE, we observed a significantly faster rate of NADH production following electrical stimulation in WT compared to MICU3-KO muscle. Taken together these data suggest that MICU3 is important for setting the threshold for $[Ca^{2+}]m$ uptake in skeletal muscle and that lack of MICU3 can impair the ability to match energy demand and supply.

There is increasing evidence that dysregulation of $[Ca^{2+}]m$ homeostasis can impact the bioenergetics of the cells and this might be a final common pathway in a multitude of disease conditions, including fatigue, lethargy, muscle myopathies (Bhosale et al., 2015; Debattisti et al., 2019; Lewis-Smith et al., 2016; Logan et al., 2014; Musa et al., 2018; Vallejo-Illarramendi et al., 2014), neurodegenerative diseases (Abeti & Abramov, 2015), models of heart failure and ischemic tissue injury (Martin & McGee, 2014; Santulli et al., 2015). Therefore, strategies that modulate $[Ca^{2+}]m$ uptake might have wide therapeutic potential. Results of this study increase our understanding of the role of MICU3 in $[Ca^{2+}]m$ regulation, and ultimately may identify MICU3 as a potential therapeutic target for the treatment of skeletal muscle diseases characterized by reduce Ca^{2+} uptake.

Supplementary Material

Refer to Web version on PubMed Central for supplementary material.

Funding

This work was funded by the NHLBI-NIH Intramural Research Program (ZO1-HL002066).

All data will be made available as required by the NIH data sharing plan.

Biography

Barbara Soledad Roman is a postdoctoral fellow in the Cardiac Physiology Laboratory located at the National Heart, Lung, and Blood Institute in Bethesda, MD. She completed her doctoral training in cardiac physiology, conducted under the guidance of Dr Cecilia Mundiña-Weilenmann and Dr Matilde Said at the National University of La Plata in Argentina. Currently, Barbara is further advancing her expertise under the mentorship of Dr. Elizabeth Murphy at the NHLBI, where she is studying the role of MICU3, mitochondrial calcium and mechanisms of cellular energy homeostasis.

Data Availability Statement, all data presented in this study have been deposited in FigShare and can be accessed via the following hyperlink. [This link can be used for review, https://figshare.com/s/b1fe03505939c0ed6f32.

When a DOI number is assigned we will link to it]

References

Abeti R, & Abramov AY (2015). Mitochondrial Ca2+ in neurodegenerative disorders. Pharmacological research, 99, 377–381. [PubMed: 26013908]

Bauer TM, & Murphy E (2020). Role of mitochondrial calcium and the permeability transition pore in regulating cell death. Circulation research, 126(2), 280–293. [PubMed: 31944918]

Baughman JM, Perocchi F, Girgis HS, Plovanich M, Belcher-Timme CA, Sancak Y, Bao XR, Strittmatter L, Goldberger O, & Bogorad RL (2011). Integrative genomics identifies MCU as an essential component of the mitochondrial calcium uniporter. Nature, 476(7360), 341–345. [PubMed: 21685886]

Bhosale G, Sharpe JA, Sundier SY, & Duchen MR (2015). Calcium signaling as a mediator of cell energy demand and a trigger to cell death. Annals of the New York Academy of Sciences, 1350(1), 107–116. [PubMed: 26375864]

Brandes R, & Bers DM (1997). Intracellular Ca2+ increases the mitochondrial NADH concentration during elevated work in intact cardiac muscle. Circulation research, 80(1), 82–87. [PubMed: 8978326]

De Stefani D, Patron M, & Rizzuto R (2015). Structure and function of the mitochondrial calcium uniporter complex. Biochim Biophys Acta, 1853(9), 2006–2011. 10.1016/j.bbamcr.2015.04.008 [PubMed: 25896525]

De Stefani D, Raffaello A, Teardo E, Szabò I, & Rizzuto R (2011). A forty-kilodalton protein of the inner membrane is the mitochondrial calcium uniporter. Nature, 476(7360), 336–340. [PubMed: 21685888]

Debattisti V, Horn A, Singh R, Seifert EL, Hogarth MW, Mazala DA, Huang KT, Horvath R, Jaiswal JK, & Hajnóczky G (2019). Dysregulation of mitochondrial Ca2+ uptake and sarcolemma repair underlie muscle weakness and wasting in patients and mice lacking MICU1. Cell reports, 29(5), 1274–1286. e1276. [PubMed: 31665639]

Denton R, Randle P, & Martin B (1972). Stimulation by calcium ions of pyruvate dehydrogenase phosphate phosphatase. Biochemical Journal, 128(1), 161. [PubMed: 4343661]

Eisner DA (2021). Pseudoreplication in physiology: more means less. Journal of General Physiology, 153(2).

Glancy B, & Balaban RS (2012). Role of mitochondrial Ca2+ in the regulation of cellular energetics. Biochemistry, 51(14), 2959–2973. [PubMed: 22443365]

Handschin C, Chin S, Li P, Liu F, Maratos-Flier E, LeBrasseur NK, Yan Z, & Spiegelman BM (2007). Skeletal muscle fiber-type switching, exercise intolerance, and myopathy in PGC-1α muscle-specific knock-out animals. Journal of Biological Chemistry, 282(41), 30014–30021. [PubMed: 17702743]

Herbison G, Jaweed M, & Ditunno J (1982). Muscle fiber types. Archives of physical medicine and rehabilitation, 63(5), 227–230. [PubMed: 6462127]

Kamer KJ, Grabarek Z, & Mootha VK (2017). High-affinity cooperative Ca2+ binding by MICU 1–MICU 2 serves as an on–off switch for the uniporter. EMBO reports, 18(8), 1397–1411. [PubMed: 28615291]

Kamer KJ, & Mootha VK (2014). MICU 1 and MICU 2 play nonredundant roles in the regulation of the mitochondrial calcium uniporter. EMBO reports, 15(3), 299–307. [PubMed: 24503055]

Kim Y, Yang DS, Katti P, & Glancy B (2019). Protein composition of the muscle mitochondrial reticulum during postnatal development. The Journal of Physiology, 597(10), 2707–2727. [PubMed: 30919448]

Lewis-Smith D, Kamer KJ, Griffin H, Childs A-M, Pysden K, Titov D, Duff J, Pyle A, Taylor RW, & Yu-Wai-Man P (2016). Homozygous deletion in MICU1 presenting with fatigue and lethargy in childhood. Neurology Genetics, 2(2).

Liu JC, Syder NC, Ghorashi NS, Willingham TB, Parks RJ, Sun J, Fergusson MM, Liu J, Holmström KM, & Menazza S (2020). EMRE is essential for mitochondrial calcium uniporter activity in a mouse model. Jci Insight, 5(4).

Liu T, & O'Rourke B (2008). Enhancing mitochondrial Ca2+ uptake in myocytes from failing hearts restores energy supply and demand matching. Circulation research, 103(3), 279–288. [PubMed: 18599868]

Logan CV, Szabadkai G, Sharpe JA, Parry DA, Torelli S, Childs A-M, Kriek M, Phadke R, Johnson CA, & Roberts NY (2014). Loss-of-function mutations in MICU1 cause a brain and muscle disorder linked to primary alterations in mitochondrial calcium signaling. Nature genetics, 46(2), 188–193. [PubMed: 24336167]

Maack C, & O'Rourke B (2007). Excitation-contraction coupling and mitochondrial energetics. Basic research in cardiology, 102, 369–392. [PubMed: 17657400]

Mammucari C, Gherardi G, Zamparo I, Raffaello A, Boncompagni S, Chemello F, Cagnin S, Braga A, Zanin S, & Pallafacchina G (2015). The mitochondrial calcium uniporter controls skeletal muscle trophism in vivo. Cell reports, 10(8), 1269–1279. [PubMed: 25732818]

Martin SD, & McGee SL (2014). The role of mitochondria in the aetiology of insulin resistance and type 2 diabetes. Biochimica et Biophysica Acta (BBA)-General Subjects, 1840(4), 1303–1312. [PubMed: 24060748]

Matesanz-Isabel J, Arias-del-Val J, Alvarez-Illera P, Fonteriz RI, Montero M, & Alvarez J (2016). Functional roles of MICU1 and MICU2 in mitochondrial Ca(2+) uptake. Biochim Biophys Acta, 1858(6), 1110–1117. 10.1016/j.bbamem.2016.02.022 [PubMed: 26903221]

Musa S, Eyaid W, Kamer K, Ali R, Al-Mureikhi M, Shahbeck N, Mesaifri FA, Makhseed N, Mohamed Z, & AlShehhi WA (2018). A middle eastern founder mutation expands the genotypic and phenotypic spectrum of mitochondrial MICU1 deficiency: a report of 13 patients. In JIMD Reports, Volume 43 (pp. 79–83). Springer. [PubMed: 29721912]

Paillard M, Csordás G, Szanda G, Golenár T, Debattisti V, Bartok A, Wang N, Moffat C, Seifert EL, & Spät A (2017). Tissue-specific mitochondrial decoding of cytoplasmic Ca2+ signals is controlled by the stoichiometry of MICU1/2 and MCU. Cell reports, 18(10), 2291–2300. [PubMed: 28273446]

Park J, Lee Y, Park T, Kang JY, Mun SA, Jin M, Yang J, & Eom SH (2020). Structure of the MICU1–MICU2 heterodimer provides insights into the gatekeeping threshold shift. IUCrJ, 7(2), 355–365.

Parks RJ, Menazza S, Holmström KM, Amanakis G, Fergusson M, Ma H, Aponte AM, Bernardi P, Finkel T, & Murphy E (2019). Cyclophilin D-mediated regulation of the permeability transition pore is altered in mice lacking the mitochondrial calcium uniporter. Cardiovascular research, 115(2), 385–394. [PubMed: 30165576]

Patron M, Granatiero V, Espino J, Rizzuto R, & De Stefani D (2019). MICU3 is a tissue-specific enhancer of mitochondrial calcium uptake. Cell Death Differ, 26(1), 179–195. 10.1038/s41418-018-0113-8 [PubMed: 29725115]

Perocchi F, Gohil VM, Girgis HS, Bao XR, McCombs JE, Palmer AE, & Mootha VK (2010). MICU1 encodes a mitochondrial EF hand protein required for Ca2+ uptake. Nature, 467(7313), 291–296. [PubMed: 20693986]

Plovanich M, Bogorad RL, Sancak Y, Kamer KJ, Strittmatter L, Li AA, Girgis HS, Kuchimanchi S, De Groot J, & Speciner L (2013). MICU2, a paralog of MICU1, resides within the mitochondrial uniporter complex to regulate calcium handling. PLoS One, 8(2), e55785. [PubMed: 23409044]

Puente, Sun J, Parks RJ, Fergusson MM, Liu C, Springer DA, Aponte AM, Liu JC, & Murphy E (2020). MICU3 Plays an Important Role in Cardiovascular Function. Circ Res, 127(12), 1571–1573. 10.1161/circresaha.120.317177 [PubMed: 33059536]

Reane DV, Vallese F, Checchetto V, Acquasaliente L, Butera G, De Filippis V, Szabò I, Zanotti G, Rizzuto R, & Raffaello A (2016). A MICU1 splice variant confers high sensitivity to the mitochondrial Ca2+ uptake machinery of skeletal muscle. Molecular Cell, 64(4), 760–773. [PubMed: 27818145]

Santulli G, Xie W, Reiken SR, & Marks AR (2015). Mitochondrial calcium overload is a key determinant in heart failure. Proceedings of the National Academy of Sciences, 112(36), 11389–11394.

Shamseldin HE, Alasmari A, Salih MA, Samman MM, Mian SA, Alshidi T, Ibrahim N, Hashem M, Faqeih E, & Al-Mohanna F (2017). A null mutation in MICU2 causes abnormal mitochondrial calcium homeostasis and a severe neurodevelopmental disorder. Brain, 140(11), 2806–2813. [PubMed: 29053821]

Siess EA, & Wieland OH (1972). Purification and Characterization of Pyruvate-Dehydrogenase Phosphatase from Pig-Heart Muscle. European Journal of Biochemistry, 26(1), 96–105. [PubMed: 4339646]

Tsai C-W, Rodriguez MX, Van Keuren AM, Phillips CB, Shushunov HM, Lee JE, Garcia AM, Ambardekar AV, Cleveland JC Jr, & Reisz JA (2022). Mechanisms and significance of tissue-specific MICU regulation of the mitochondrial calcium uniporter complex. Molecular Cell, 82(19), 3661–3676. e3668. [PubMed: 36206740]

Vallejo-Illarramendi A, Toral-Ojeda I, Aldanondo G, & de Munain AL (2014). Dysregulation of calcium homeostasis in muscular dystrophies. Expert reviews in molecular medicine, 16, e16. [PubMed: 25293420]

Vecellio Reane D, Cerqua C, Sacconi S, Salviati L, Trevisson E, & Raffaello A (2022). The Splicing of the Mitochondrial Calcium Uniporter Genuine Activator MICU1 Is Driven by RBFOX2 Splicing Factor during Myogenic Differentiation. International Journal of Molecular Sciences, 23(5), 2517. [PubMed: 35269658]

Wang H, Yang H, Shivalila CS, Dawlaty MM, Cheng AW, Zhang F, & Jaenisch R (2013). One-step generation of mice carrying mutations in multiple genes by CRISPR/Cas-mediated genome engineering. cell, 153(4), 910–918. [PubMed: 23643243]

Watanabe D, & Wada M (2020). Fatigue-induced change in T-system excitability and its major cause in rat fast-twitch skeletal muscle in vivo. The Journal of Physiology, 598(22), 5195–5211. [PubMed: 32833287]

Wescott AP, Kao JP, Lederer WJ, & Boyman L (2019). Voltage-energized calcium-sensitive ATP production by mitochondria. Nature Metabolism, 1(10), 975–984.

Westerblad H, & Allen D (1991). Changes of myoplasmic calcium concentration during fatigue in single mouse muscle fibers. The Journal of general physiology, 98(3), 615–635. [PubMed: 1761971]

Willingham TB, Zhang Y, Andreoni A, Knutson JR, Lee DY, & Glancy B (2019). MitoRACE: evaluating mitochondrial function in vivo and in single cells with subcellular resolution using multiphoton NADH autofluorescence. The Journal of Physiology, 597(22), 5411–5428. [PubMed: 31490555]

Xing Y, Wang M, Wang J, Nie Z, Wu G, Yang X, & Shen Y (2019). Dimerization of MICU Proteins Controls Ca(2+) Influx through the Mitochondrial Ca(2+) Uniporter. Cell Rep, 26(5), 1203–1212.e1204. 10.1016/j.celrep.2019.01.022 [PubMed: 30699349]

Yang Y-F, Yang W, Liao Z-Y, Wu Y-X, Fan Z, Guo A, Yu J, Chen Q-N, Wu J-H, & Zhou J (2021). MICU3 regulates mitochondrial Ca2+-dependent antioxidant response in skeletal muscle aging. Cell death & disease, 12(12), 1–13. [PubMed: 33414393]

Key Points

- Mitochondrial calcium uptake is an important regulator of bioenergetics and cell death and is regulated by the mitochondrial calcium uniporter (MCU) and 3 calcium sensitive regulatory proteins (MICU1,2 and 3).
- Loss of MICU3 leads to impaired exercise capacity and decreased time to skeletal muscle fatigue.
- Skeletal muscle from MICU3-KO mice exhibits a net oxidation of NADH during electrically stimulated muscle contractions, suggesting that MICU3 plays a role in skeletal muscle physiology by matching energy demand and supply.

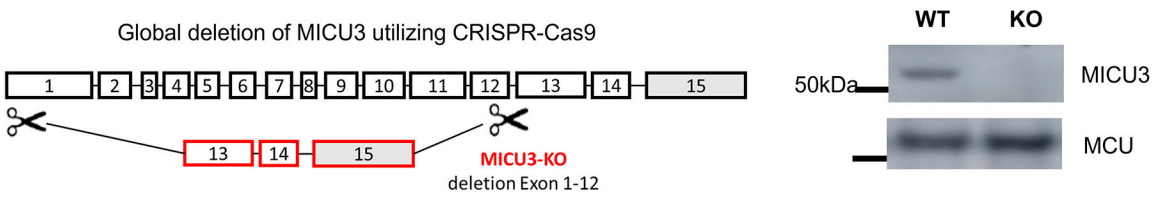

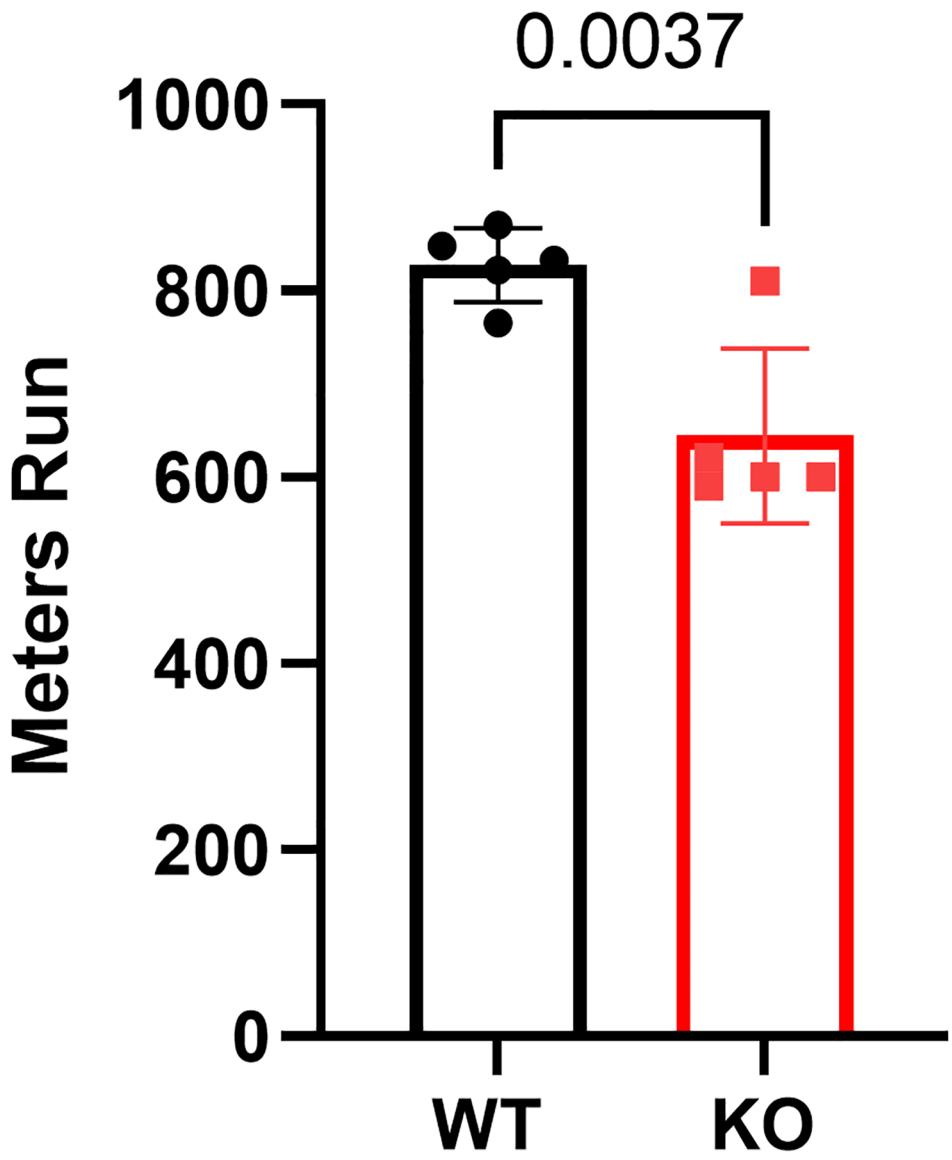

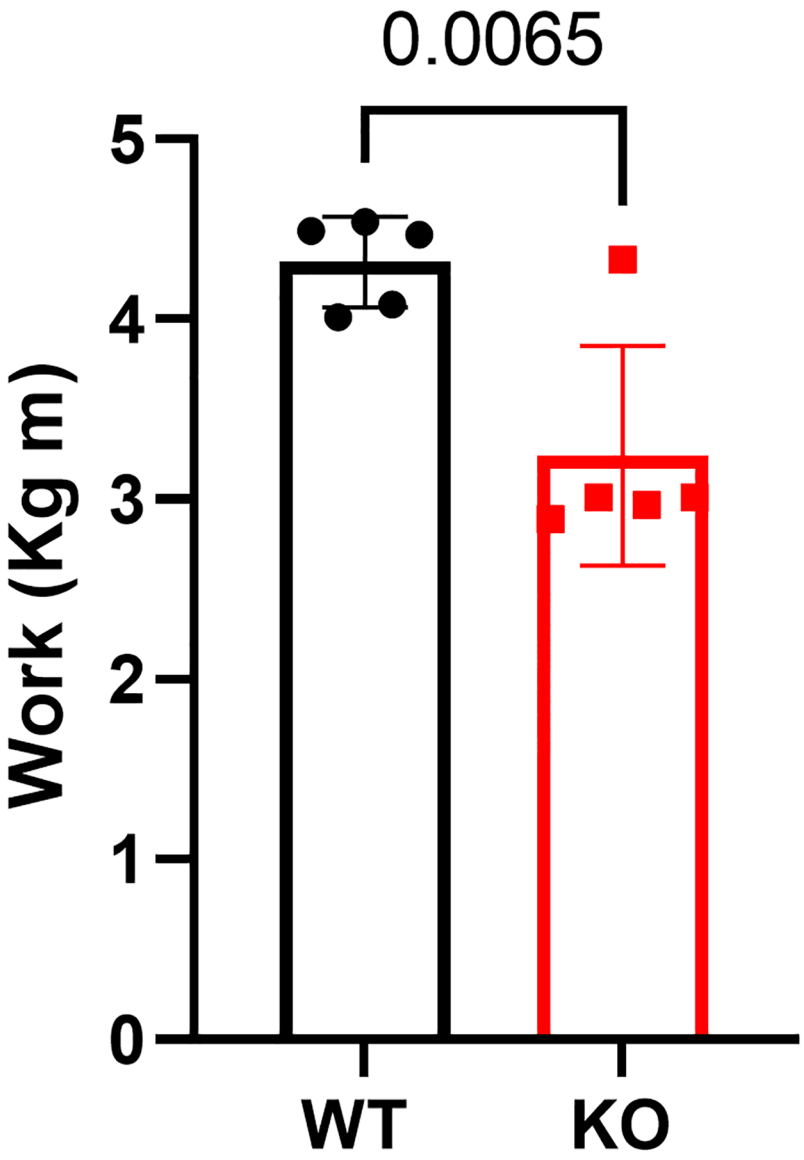

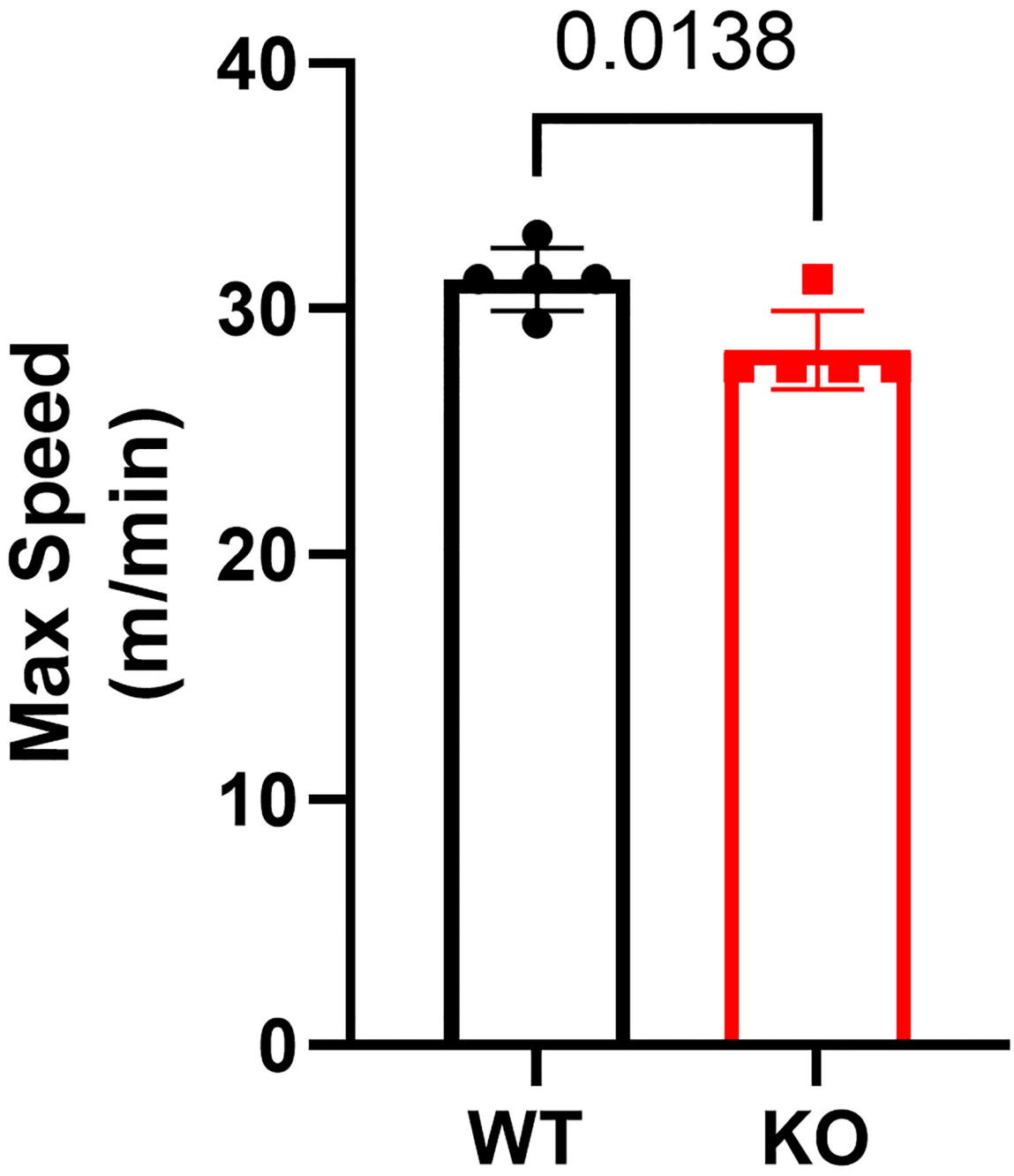

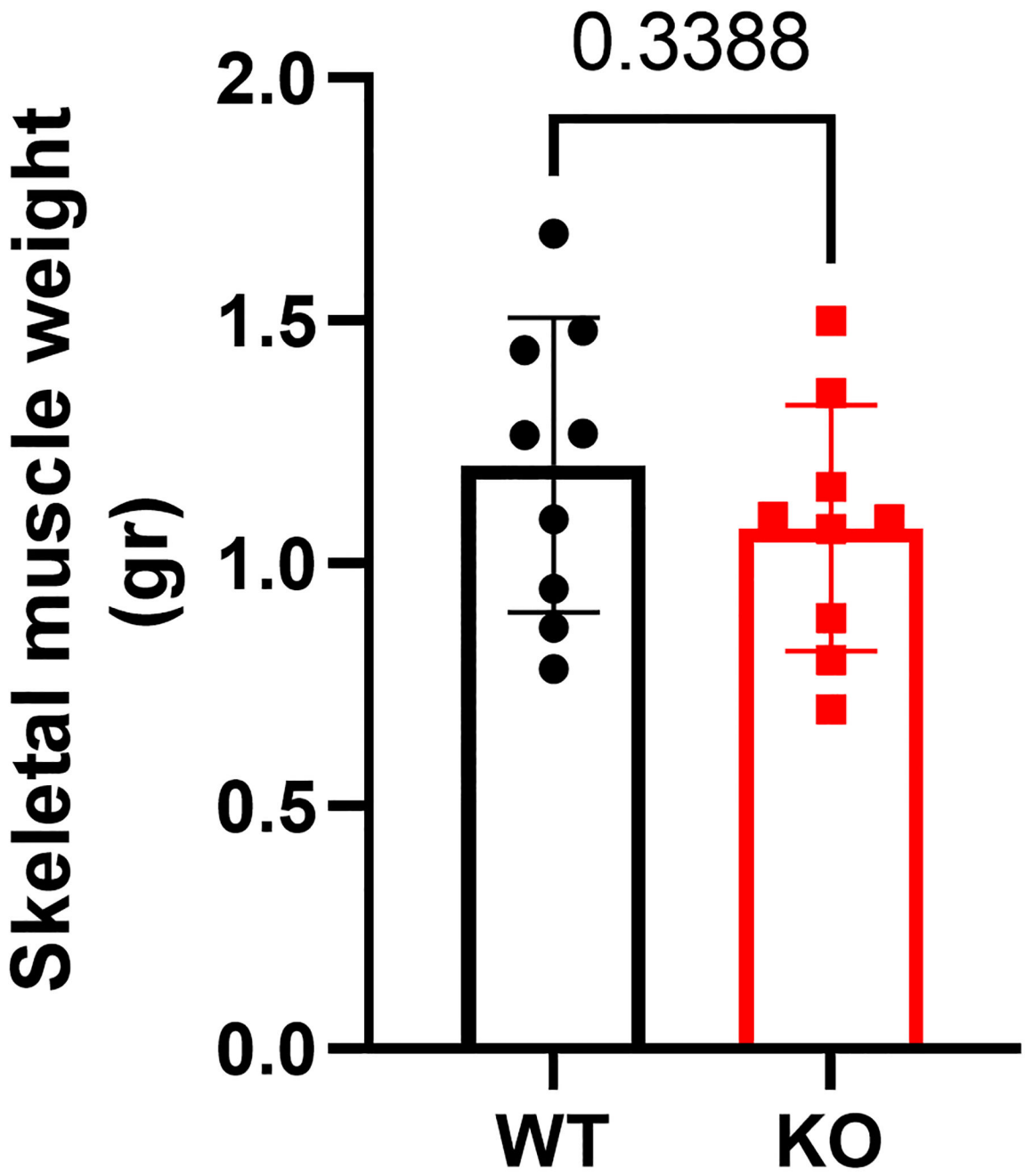

Figure 1. Loss of MICU3 impaired exercise capacity.

A) Scheme of the MICU3 gene with the composition of exons and targeted deletion of exons 1 to 12 mediated by CRISPR-Cas9. Exons 1 through 14 encompass the coding sequence, whereas exon 15 is noncoding. The scissors indicate the targeting sites for the CRISPR short guide RNAs. On the right is a WB from soleus muscle demonstrating no expression of MICU3 in KO mice. Exercise testing showed MICU3-KO mice have diminished B) distance traveled expressed in meter and C) work expended during exercise. This correlates with much shorter D) speed during excise. E) Differences were not due to a reduce in the mass

of skeletal muscle (hind limb muscles from both legs) in the MICU3-KO. (n = 5–10 per genotype, data are represented as mean ± SD, and significance was assessed using t-test).

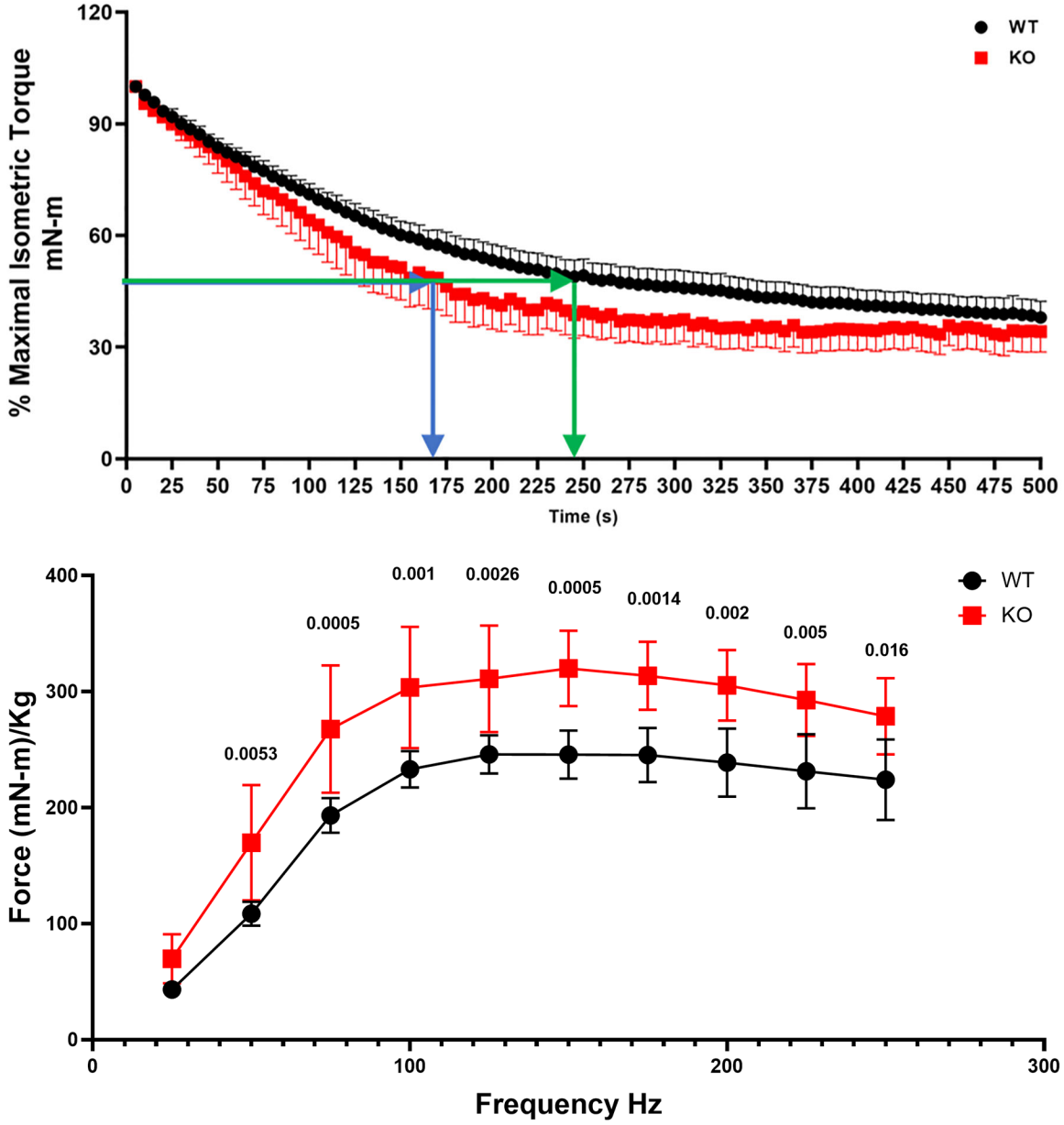

Figure 2. Loss of MICU3 altered torque and fatigue.

A series of successive tetanic contractions were applied to the muscle (GAS and soleus) to induce muscle fatigue expressed as A) Maximal Isometric Torque vs Time expressed in seconds from WT and MICU3-KO mice. B) Specific Torque was used to measure the kinetic response from mechanical force of the muscle *in-vivo* for each stimulation frequency from 25–250 Hz. (n = 5 per genotype, data are represented as mean ± SD , and significance was assessed using one-way ANOVA)

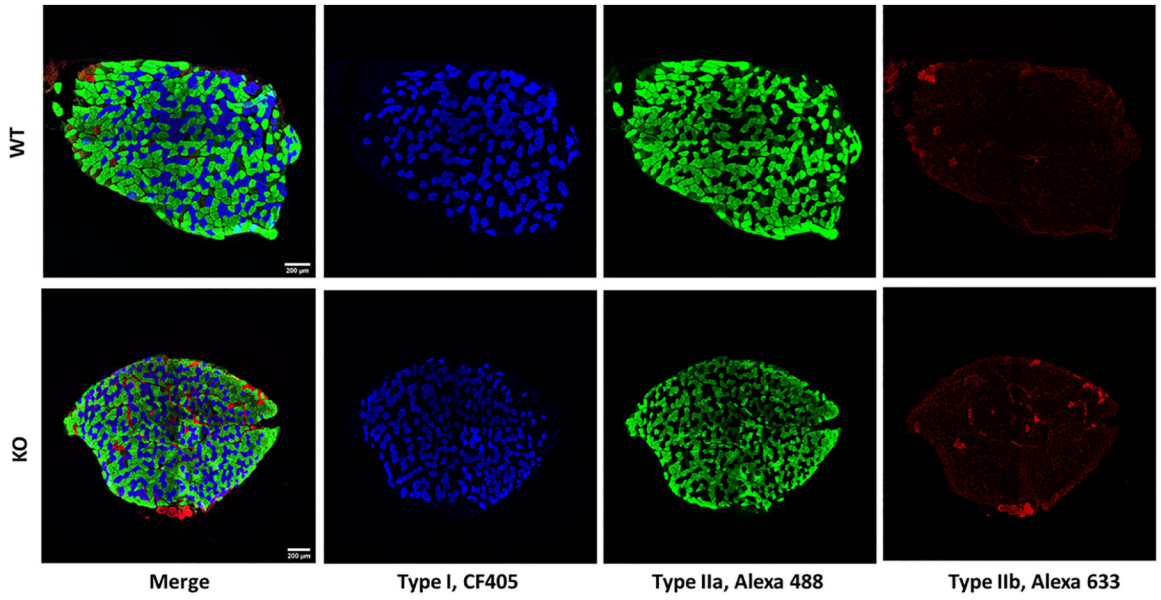

B) EDL

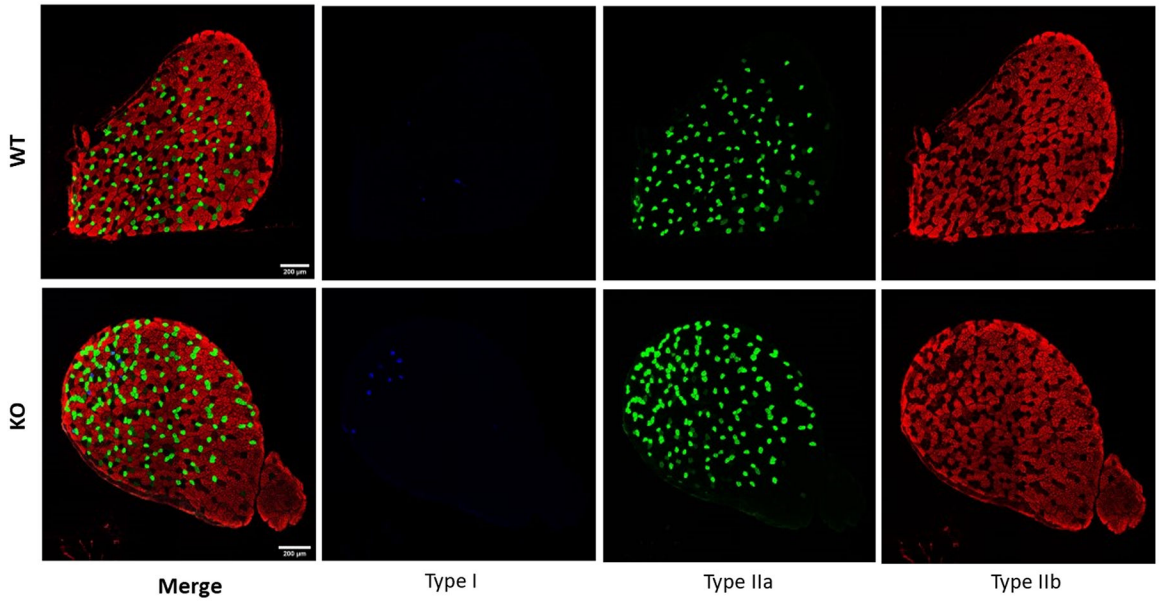

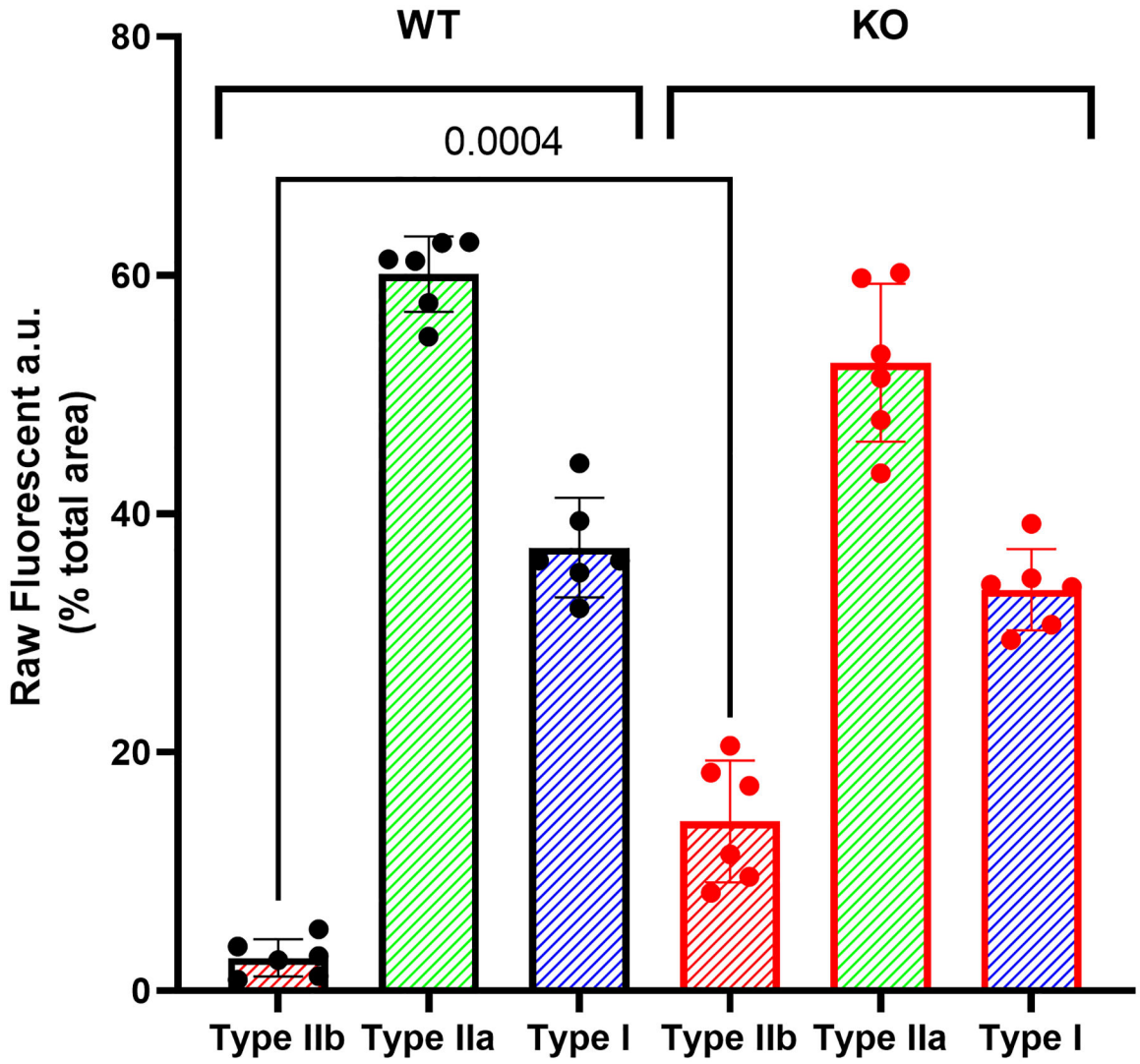

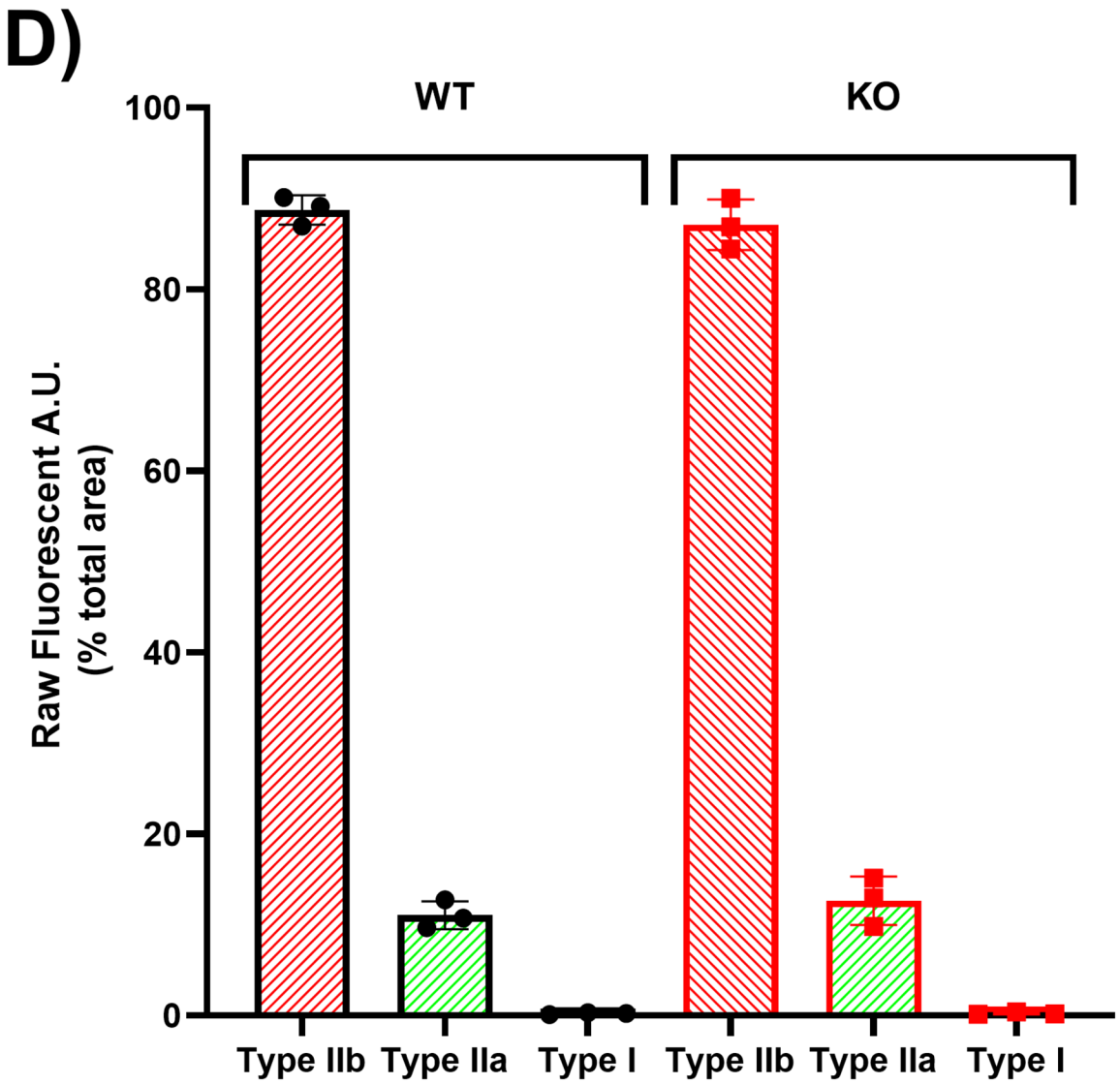

Figure 3. Lack of MICU3 triggered fiber type switching.

Confocal image of a section of the soleus in A) and EDL in B) from WT on the upper panel and KO mice at the bottom. The cryo-section of soleus and EDL were immune stained for the different type of fibers. Type I: Blue, CF405 Myosin Heavy Chain Type I Antibody. Type IIa: Green, Alexa 488 -Myosin Heavy Chain Type IIA Antibody. Type IIb: Red, Alexa 633 Myosin Heavy Chain Type IIB Antibody. Bar graph of soleus in C) and ELD in D) quantification of raw fluorescent as a percentage of the total area of the fiber section (n = 3–6 per genotype, data are represented as mean ± SD, significance was assessed using t-test).

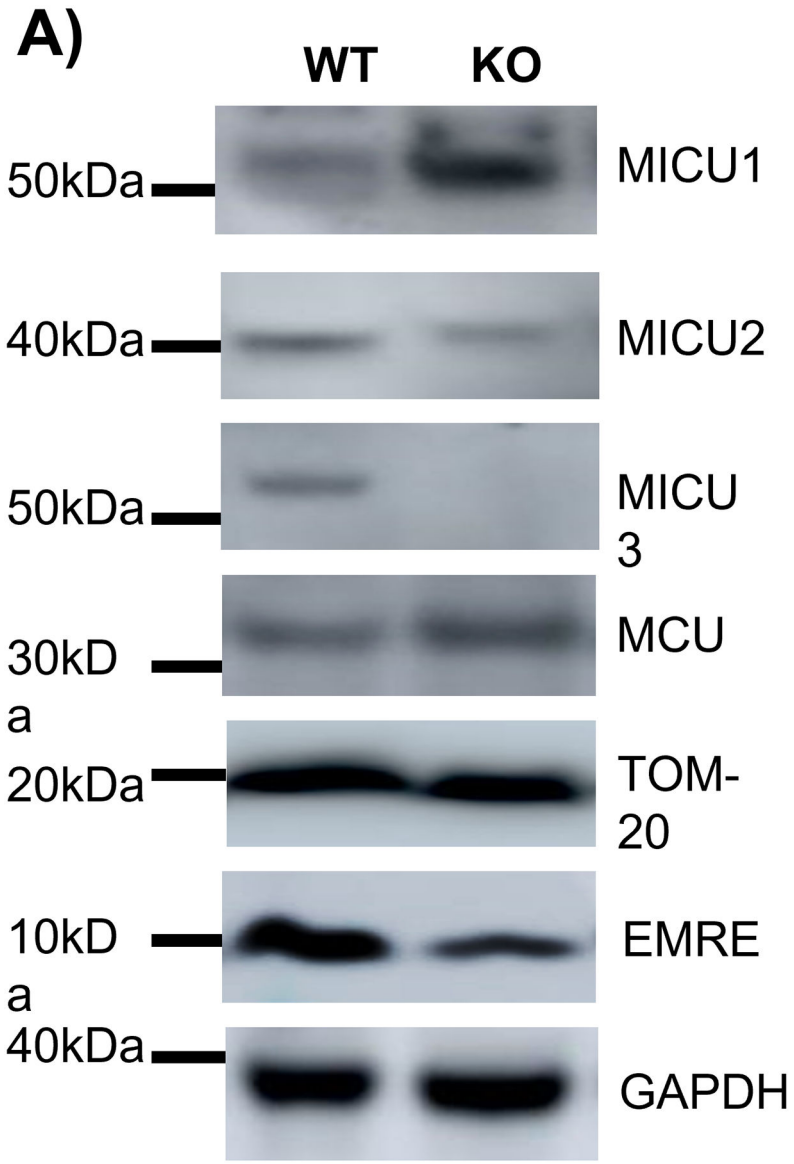

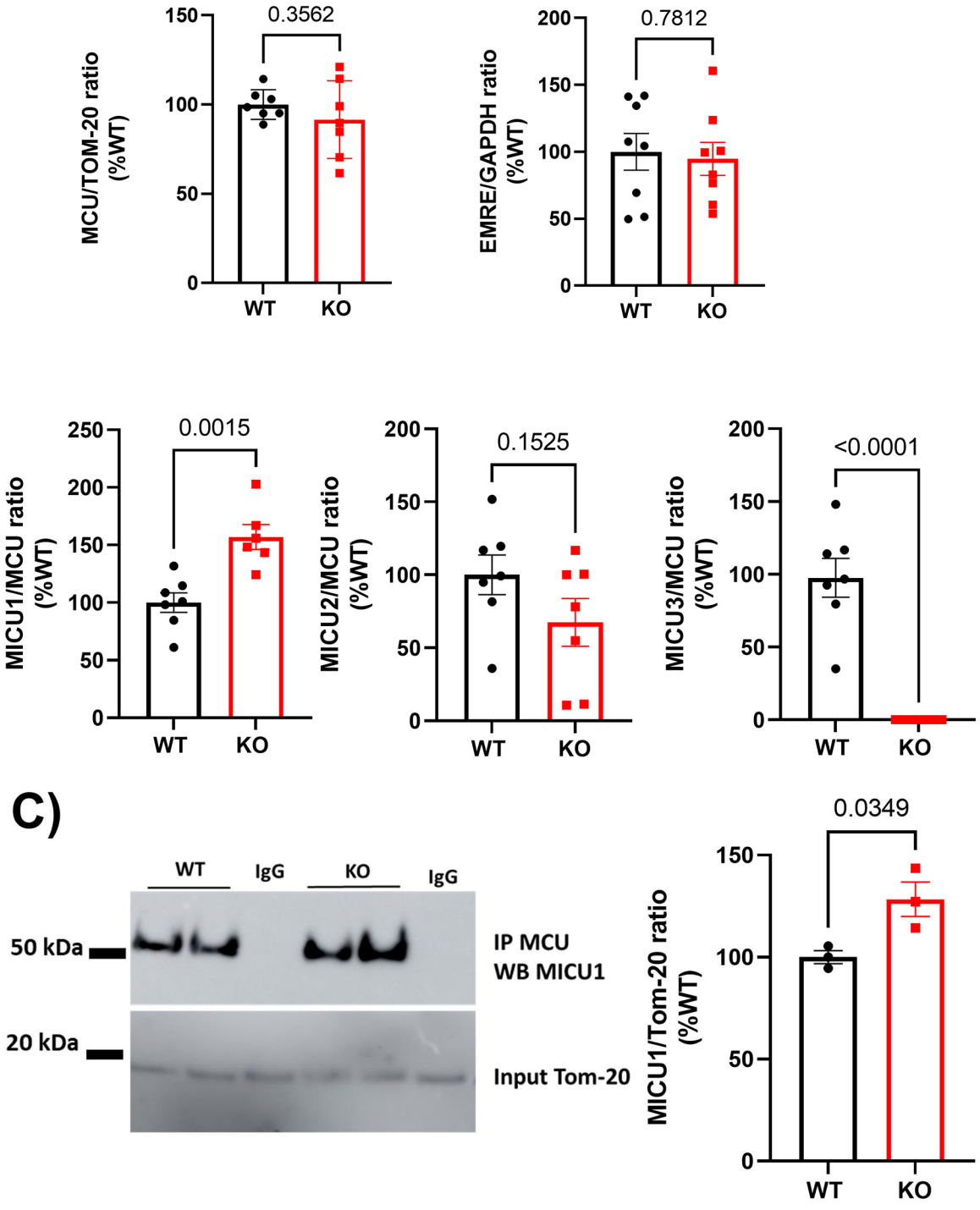

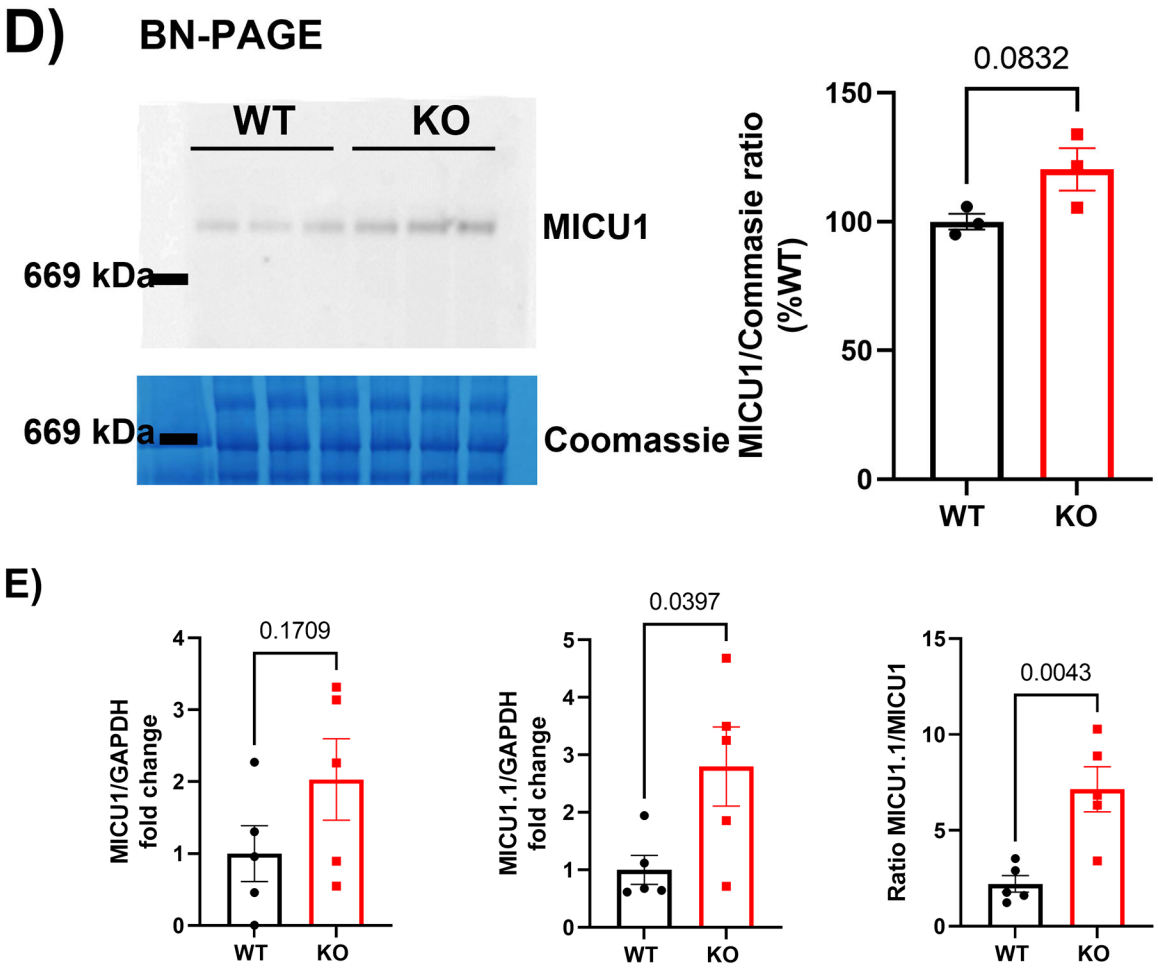

Figure 4. MICU1.1 is upregulated in the skeletal muscle of MICU3-KO mice.

Western blot analysis of MICU1, MICU2, MICU3, MCU, EMRE, GAPDH and TOM-20 protein expression in isolated soleus muscle from WT and MICU3-KO. A) Western blot of MICUs, MCU, TOM-20, EMRE and GAPDH. Molecular weights from the protein ladder are indicated on the left. B) Total protein expression of MCU was normalized to TOM-20 and compared between WT and MICU3-KO mice. MICU1, 2 and 3 were normalized to MCU and EMRE was normalized to GAPDH because of its close MW to TOM-20 (n = 7 per genotype, data are represented as mean ± SD, and significance was assessed using t-test). C) The MCU complex from a mitochondrial enriched fraction derived from mouse WT and MICU3-KO skeletal muscle was immunoprecipitated with anti-MCU antibody. The precipitated proteins were immunoblotted with MICU1 antibody (n = 3 per genotype). D) Representative BN-PAGE gel run using a freshly mitochondrial enriched fraction derived from mouse skeletal muscle of WT and MICU3-KO. The gel was immunoblotted with anti-MICU1 antibody (Data are representative of at n = 3 biological replicates). E) Quantitative PCR (SYBR) was performed from the RNA fractions of WT and MICU3-KO soleus muscle. (n = 5 per genotype, data are represented as mean ± SD and significance was assessed using t-test).

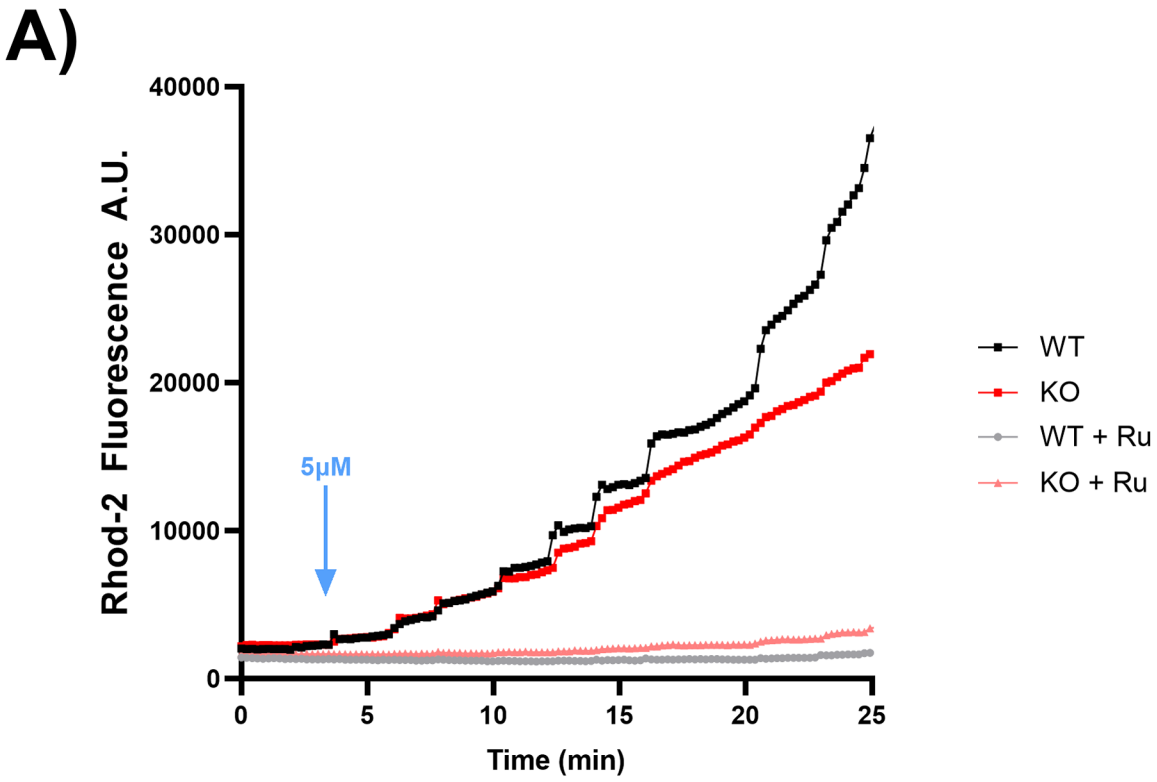

B)

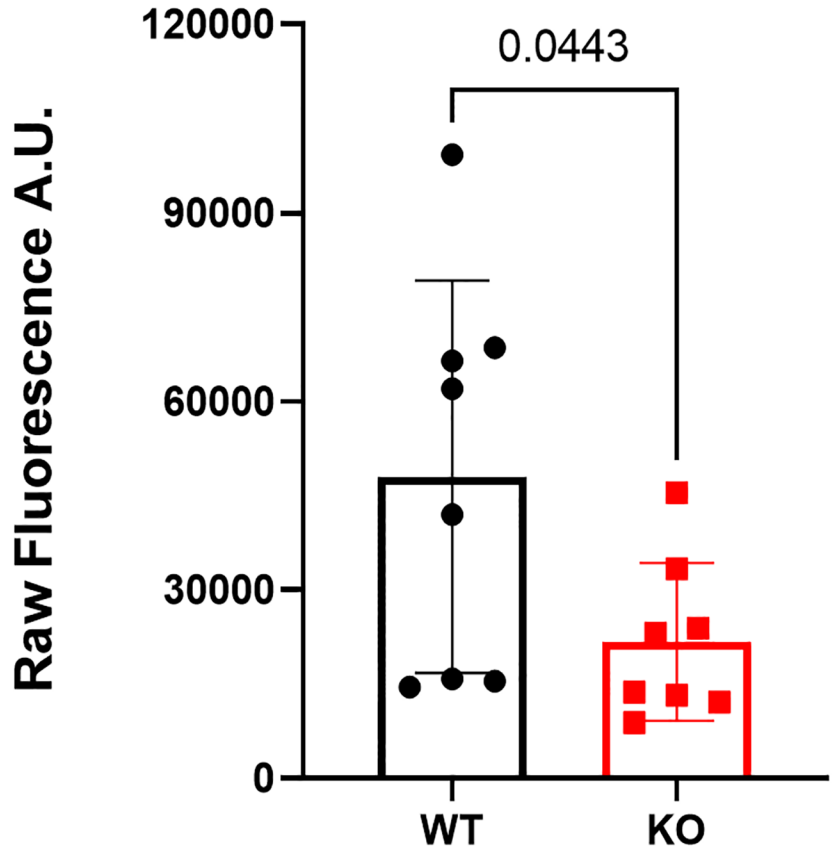

C)

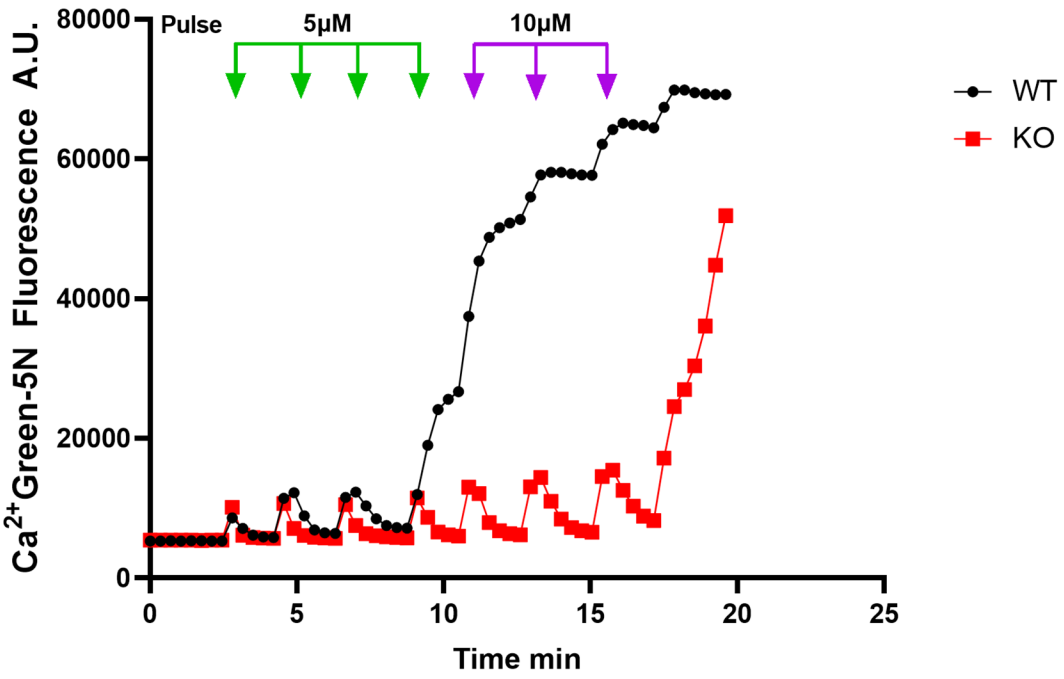

D)

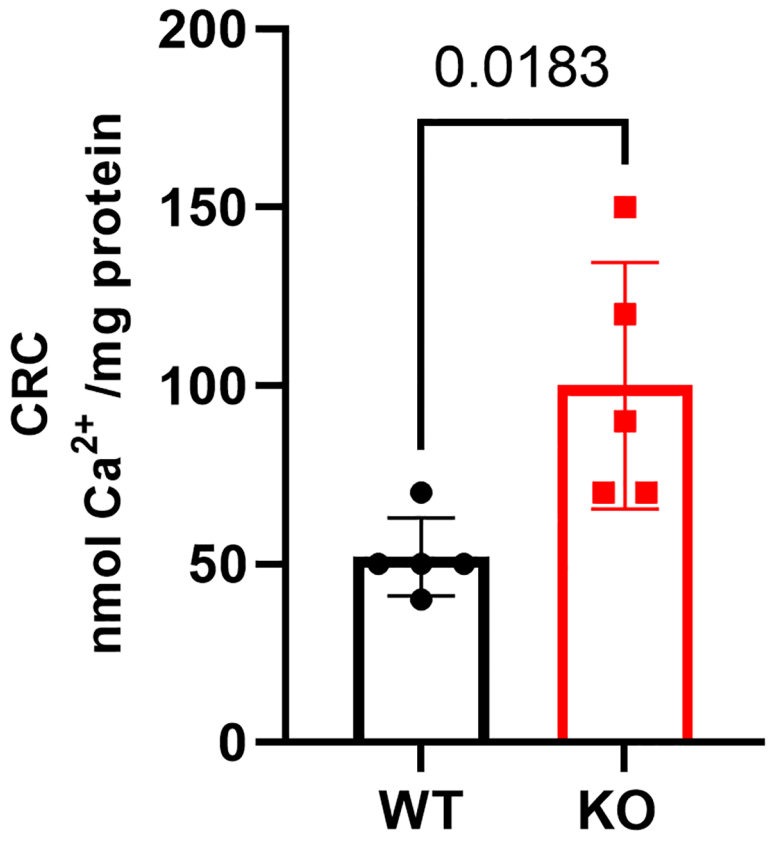

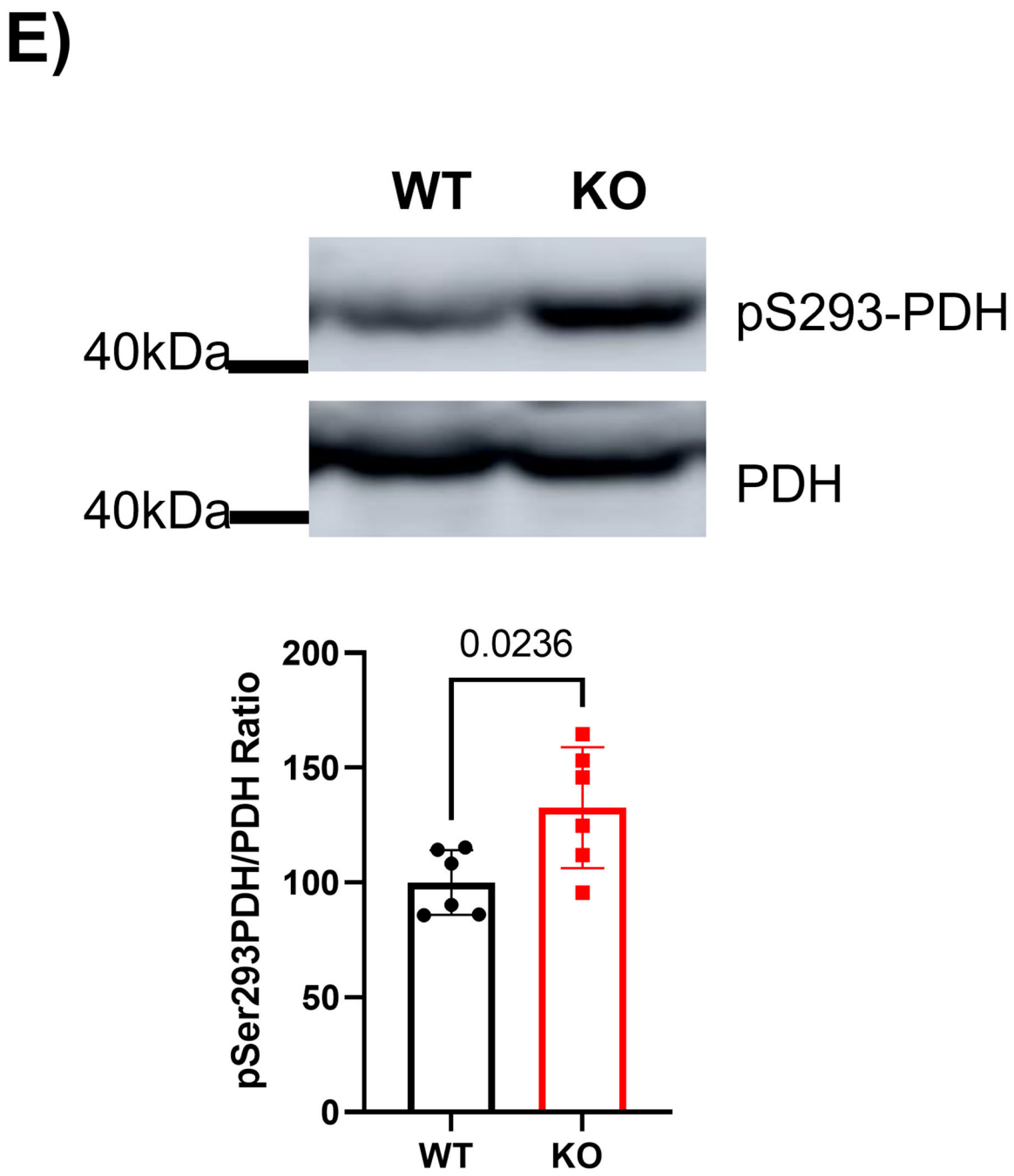

Figure 5. Loss of MICU3 reduces mitochondrial calcium uptake.

A) Representative mitochondrial Ca^{2+} uptake measured using Rhod-2, which was loaded into the matrix of WT and MICU3-KO skeletal muscle mitochondria. 5 μM pulses of Ca^{2+} were added. B) Bar graph of quantification of Ca^{2+} uptake Rhod-2 fluorescence measured at the end of experiment. C) Representative CRC traces from WT and MICU3-KO performed using Ca^{2+} Green-5N. 5 and 10 μM pulses of Ca^{2+} were added until the opening of the PTP. D) Bar graph of quantification pulses of Ca^{2+} added to open PTP. E) Western Blot analysis of phosphorylated-(293)-Ser PDH (pyruvate dehydrogenase) expression top panel and total

PDH which served as a loading control in bottom panel from soleus muscle of WT and MICU3-KO. Molecular weights from the protein ladder are indicated on the left. (n = 5–8 per genotype, data are represented as mean ± SD and significance was assessed using t-test).

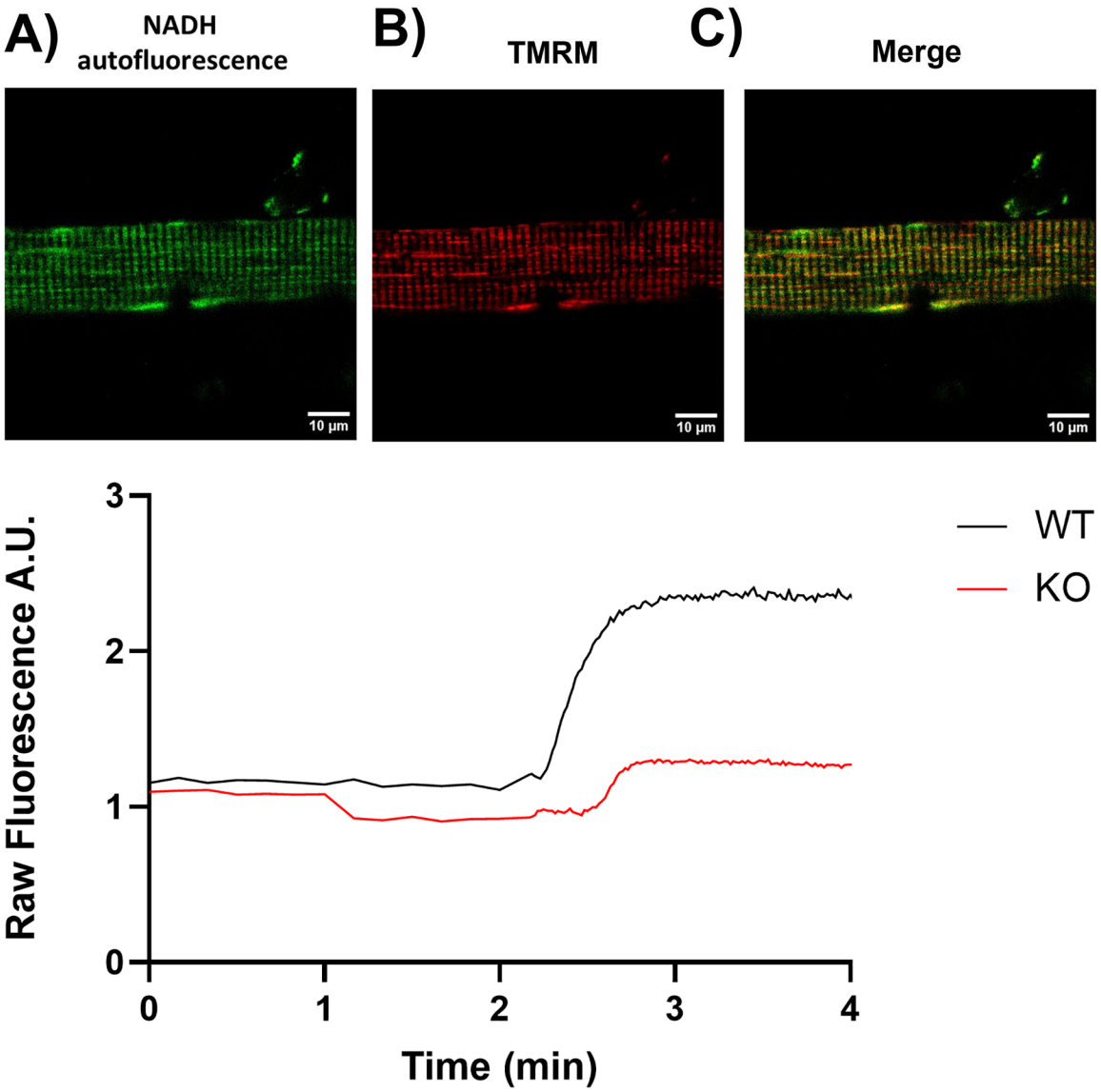

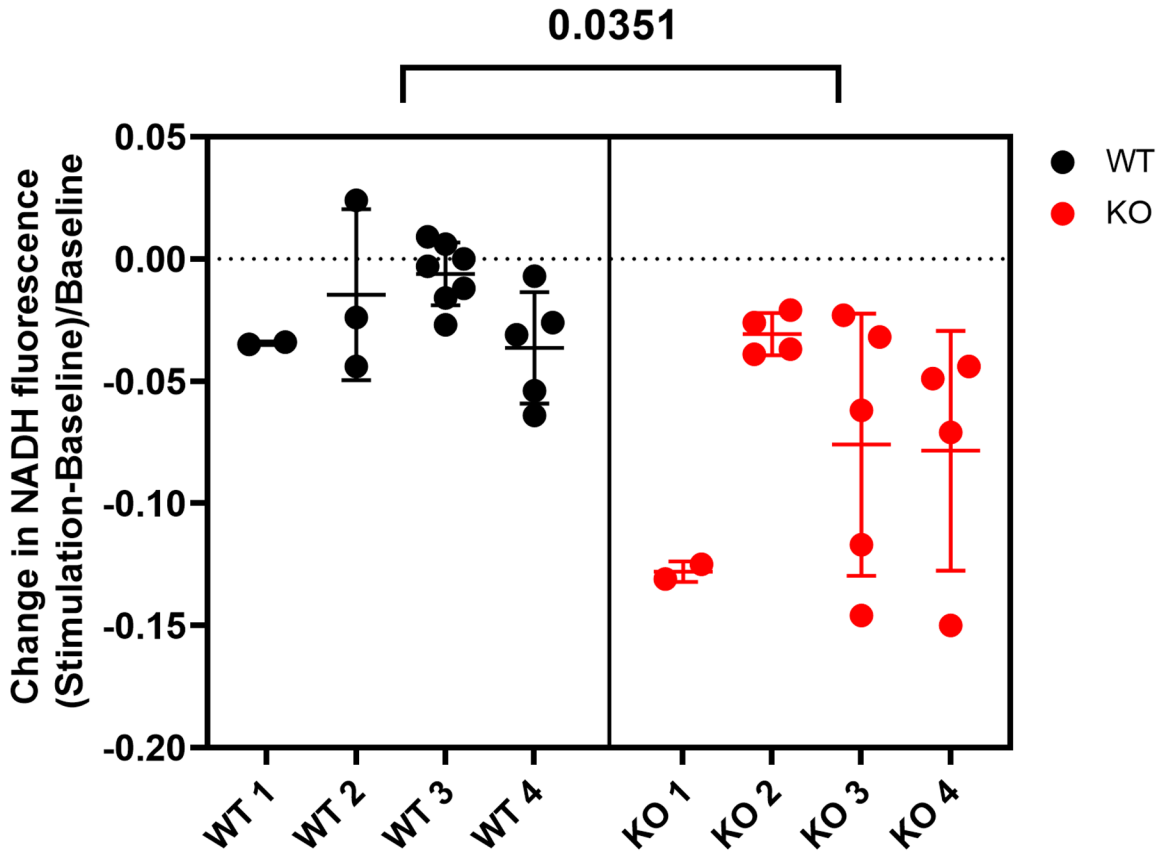

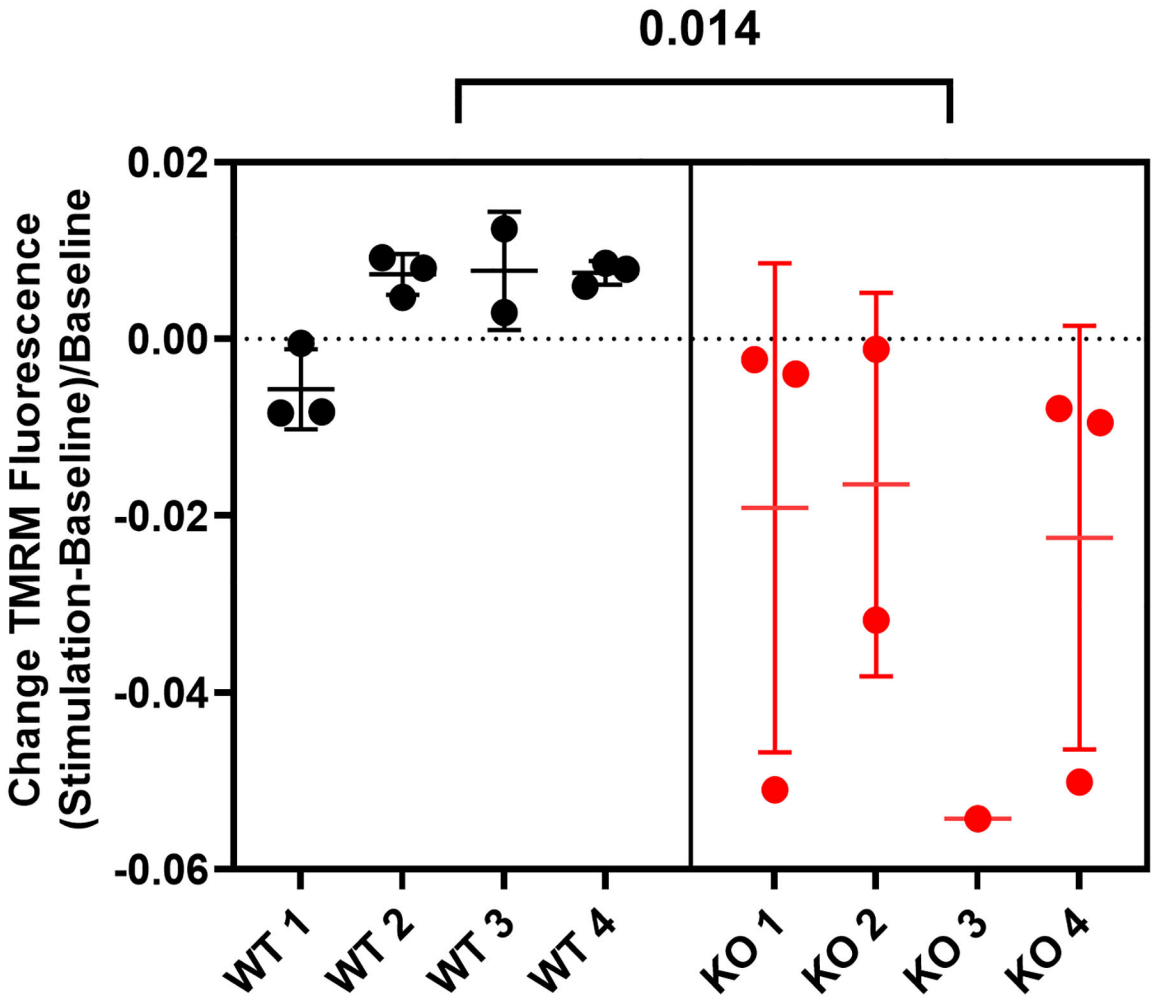

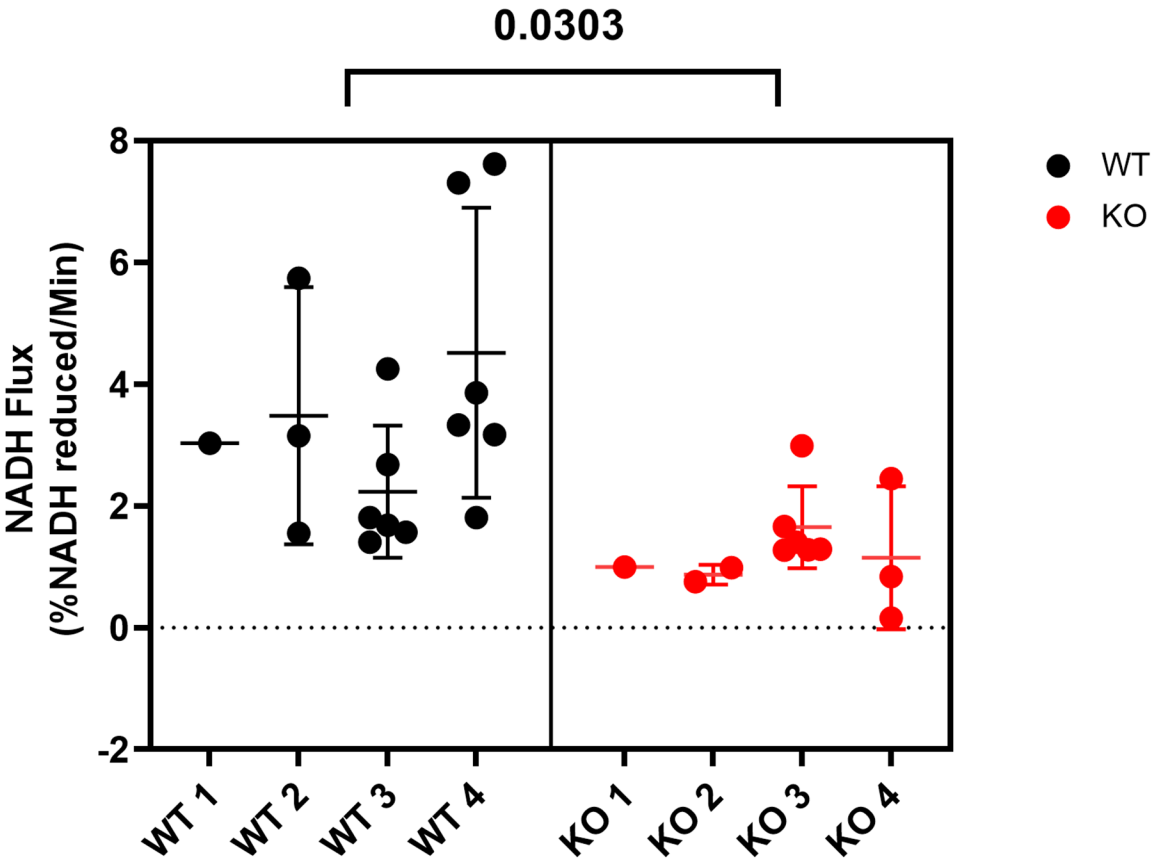

Figure 6. MICU3-KO fibers have reduced generation of NADH.

A) One-photon microscopy of endogenous mitochondrial NADH auto fluorescence in isolated fiber of soleus muscle from WT and MICU3-KO mice. B) Mitochondrial membrane potential measured with TMRM and C) Colocalization (Merge). D) Representative trace of NADH autofluorescence at baseline, post-stimulation and after inhibition of oxidative phosphorylation via perfusion of 5 mM cyanide (CN^-) in WT and MICU3-KO fibers. E) Change in NADH fluorescence response of the individual fibers during stimulation compared to baseline, calculated as $\Delta F/F_0$ (Stimulation-Baseline)/Baseline. F) Changes in TMRM fluorescence of individual fibers during stimulation compared to baseline, calculated as ratio between TMRM fluorescence and total NADH reduced (Stimulation-Baseline)/ Baseline. G) Rate of increase in NADH fluorescence measured using mitoRACE (Slope). (Cells n=9–17 corresponding to 4 individual mice per genotype, data are represented as mean ± SD, and significance was assessed using nested t-test).

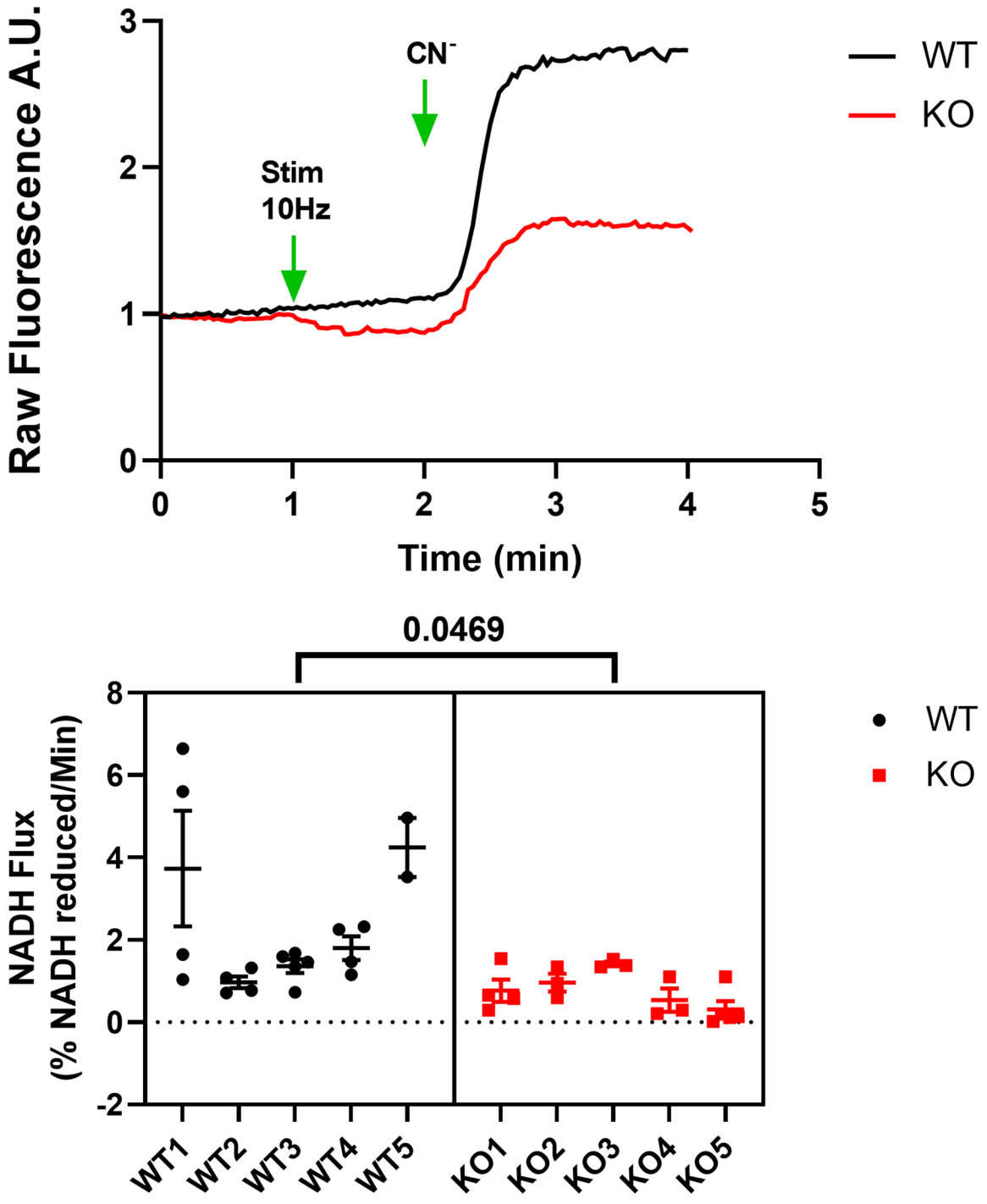

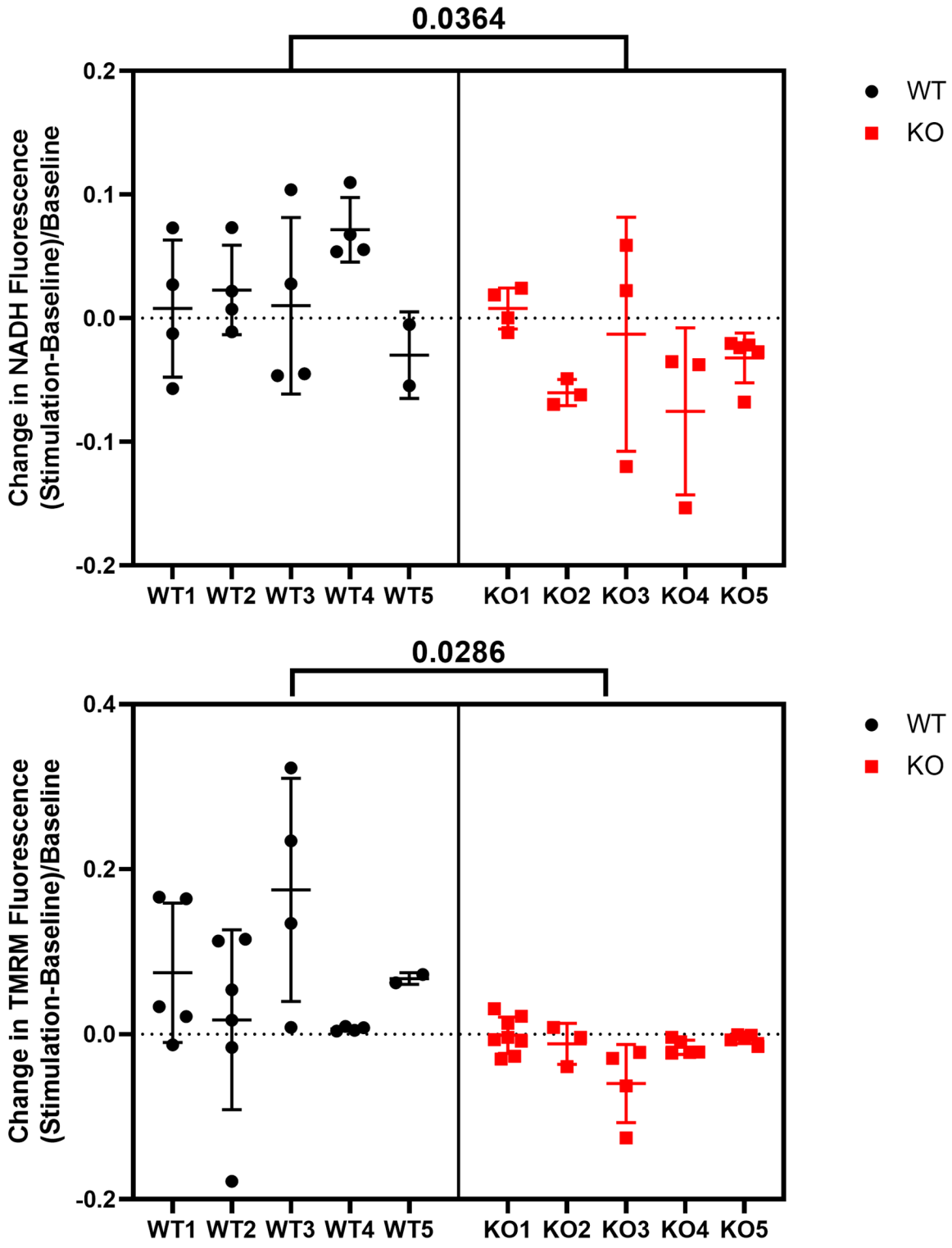

Figure 7. MICU3-KO FDB fibers have reduced generation of NADH.

A) Representative trace of NADH autofluorescence at baseline, post-stimulation and after inhibition of oxidative phosphorylation via perfusion of 5 mM cyanide (CN^-) in WT and MICU3-KO FDB fibers. B) Rate of increase in NADH fluorescence measured using

mitoRACE (Slope). C) Change in NADH fluorescence response of the individual FDB fibers during stimulation compared to baseline, calculated as $\Delta F/F_0$ (Stimulation-Baseline)/Baseline. D) Changes in TMRM fluorescence of individual fibers during stimulation compared to baseline, calculated as ratio between TMRM fluorescence and total NADH reduced (Stimulation-Baseline)/Baseline. (Cells n=18–23 corresponding to 5 individual mice per genotype, data are represented as mean ± SD, and significance was assessed using nested t-test).